university of groningen / faculty of science and engineering / mathematics and applied mathematics

An Application of Filippov Systems to Model Discontinuous Harvesting in a Predator-Prey Model

Bachelor's Project Mathematics

July 2018

Student: J. Norden

First supervisor: Prof. dr. H. Waalkens

Second assessor: Dr. I. Hoveijn

Abstract

Harvesting of the predators is introduced to a Rosenzweig-MacArthur predator-prey model whenever the population density of the predators exceeds a certain threshold value. This introduces a discontinuity along the threshold value in the vector field describing the dynamics. A continuous version of the Rosenzweig-MacArthur model is discussed in detail. It follows an introduction to the theory of Filippov systems and discontinuity-induced bifurcations. These are bifurcations that arise due to interactions with the line of discontinuity in the vector field. Finally, the theory is applied to the case of a one parameter family of Filippov systems which is based on the Rosenzweig-MacArthur model and describes the population-density-dependent harvesting. It is found that due to interactions with the discontinuity line, there exist parameter intervals where there are two attractors. This is a significant change in the behaviour of solutions to this system since the continuous version of the predator-prey model only allows for a single attractor at all times. It is concluded that population-density-dependent harvesting could be used to stabilize sensible ecosystems that exhibit potentially dangerous excursions of periodic solutions which come close to the coordinate axes.

Contents

1 Introduction

In the resource supply chains, large amounts of the worlds population rely on our ability to exploit natural resources without diminishing them to a degree from which they cannot recover. The entirety of the fishing industry as well as the lumber industry are examples. The consistent harvesting of natural resources has a long history to be modeled by predator-prey models. The Rosenzweig-MacArthur model is commonly used to describe idealized interactions of predator and prey populations. In a modified version of this model, harvesting of the predator population is only active when the predators are abundant, i.e. when the population of predators is above a certain threshold value. This splits the phase space of the system at hand into two regions, which are separated at the threshold value. On each region the dynamics are described by different vector fields. This introduces a discontinuity along the threshold value. The described system belongs to the family of so called Filippov systems.

In general Filippov systems are piecewise smooth dynamical systems, i.e. they are dynamical systems for which the phase space is partitioned into, possibly many, different regions. On each of those regions the governing equations are different. In the context of this paper, the systems are assumed to be continuous-time systems, as the focus lies on the application to predator-prey models. The main purpose of this thesis is to perform a bifurcation analysis on a modified Rosenzweig-MacArthur model and interpret how different modes of harvesting affect the long term evolution of these predator and prey populations. To do so a classification of bifurcations in Filippov is needed. Such a bifurcation theory for Filippov systems has been developed by Kuznetsov, Rinaldi and Gragnani[8]. Their results will be used to perform the bifurcation analysis presented in this thesis. The reader is expected to be familiar with the basic concepts of dynamical systems theory. However, a selection of key prerequisites will be treated in the appendix.

Motivation and Aims

Predator-prey models are a potent mean to describe a multitude of processes surrounding us. These models do not restrict to the classical "fox-eats-rabbit" scenario: Today, complex processes ranging from resource-consumer interactions in economy to tumor cell-immune system interactions in medicine are being modeled using the basic principles of predator-prey systems. Due to this massive spectrum of applications, it is essential to keep improving these models and make them more realistic while keeping their complexity to a minimum. This is where the population-density-dependent harvesting in the modified Rosenzweig-MacArthur model comes in. It represents a way of including a simple kind of control one can exert on such interactions. As we will see later on, these simple changes can have a big influence on the system dynamics and could help minimizing the risk of species going extinct.

This thesis aims to familiarize the reader with the Rosenzweig-MacArthur predator-prey model as well as the basic notions of planar Filippov systems that will be needed to model population-density-dependent harvesting. Further, a selection of bifurcations that occur in planar Filippov systems will be presented. Finally, a one parameter family of Filippov systems will be introduced to model the population-density-dependent harvesting in a modified version of a Rosenzweig-MacArthur

model. It is aimed to replicate findings from article [8]. The results that are to be replicated concern the bifurcation analysis of a Rosenzweig-MacArthur type model with a certain parameter configuration. Further, a second parameter configuration generating a qualitatively different class of phase portraits will be examined in the same manner. Finally, the results are to be compared and interpreted with regard to their ecological context.

The thesis is structured as follows: In Chapter 2, the Rosenzweig-MacArthur model is introduced and its main characteristics presented. Basic notions for Filippov systems are discussed in chapter 3. In chapter 4 the reader will be introduced to the bit of bifurcation theory for Filippov systems that is necessary to examine the modified Rosenzweig-Macarthur model. Chapter 5 contains the bifurcation analysis on the modified Rosenzweig-Macarthur model and the main results of this thesis. Finally, chapter 6 contains a discussion of the results.

2 The Rosenzweig MacArthur Model

2.1 Introduction to the model

The Rosenzweig MacArthur model is a system of two differential equations that describes the interactions of a predator and a prey population. The results presented and elaborated on in this chapter are taken from an article by H.L. Smith [10]. The density of the prey population is given by x_1 and the density of the predator population is given by x_2. Typically, predator-prey models are of the form

$$\begin{aligned}\dot{x}_1 &= \text{birth rate - natural death rate of prey - kill rate,}\\ \dot{x}_2 &= \text{reproduction rate - natural death rate of predators.}\end{aligned}$$

The next question is now how to find specific terms that describe, for example, the birth rate of the prey or the reproduction rate of the predators. These mathematical descriptions should model the real life behaviour sufficiently well, while at the same time being of simple forms. Ideally, these models are so simple that great insight about the behaviour of solutions can be gained from purely analytic investigation. The following are commonly made choices:

1. The prey has a logistic growth and death rate in the absence of predators.
2. The predators have a linear death rate.
3. The predators do not interfere with each other when hunting, hence the rate at which predators kill prey is linear with respect to the predator density.
4. The predator reproduction rate is proportional to the rate at which predators kill prey.

Translating these assumptions into system equations yields the following system:

$$\begin{cases}\dot{x}_1 = rx_1(1-\frac{x_1}{K}) - x_2h(x_1)\\ \dot{x}_2 = x_2\big[dh(x_1) - c\big]\end{cases} \tag{1}$$

The parameter r represents the reproduction rate of the prey, while K is their carrying capacity. The function $h(x_1)$ represents the per-predator kill rate. The death rate of the predators is given by c, while their reproduction rate is represented by d. Note that r, K, c and d are positive. In this thesis h is assumed to be given by

$$h(x_1) = \frac{sx_1}{1+s\tau x_1}$$

which is also known as the Holling type II functional response. A derivation of this functional response can be found in chapter 4 of P. Turchin's book *Complex Population Dynamics* [11]. The parameter s represents the rate at which a predator searches for prey in units of area per unit time. The time it takes a predator to handle prey, i.e. kill, devour and rest, is described by τ. Both s and τ are positive.

2.2 Rescaling

The system as it is has 6 parameters. In what follows, the variables and parameters will be rescaled to arrive at an equivalent system with only 3 parameters. This will greatly simplify further analysis. Consider system (1). Introduce

$$u = x_1/X \text{ and } v = x_2/Y,$$

where $X, Y > 0$ are to be chosen conveniently. The differential equations for u and v are then as follows:

$$\dot{u} = \dot{x}_1/X = ru(1 - \frac{uX}{K}) - \frac{sYuv}{1 + s\tau Xu},$$
$$\dot{v} = \dot{x}_2/Y = \frac{sdXuv}{1 + s\tau Xu} - cv.$$

Now pick $X = K$ and $Y = dX = dK$. Why this choice is convenient will become evident soon. Substituting for X and Y and rearranging, the system becomes

$$\dot{u} = ru(1 - u) - \frac{\frac{d}{\tau}uv}{\frac{1}{s\tau K} + u},$$
$$\dot{v} = \frac{\frac{d}{\tau}uv}{\frac{1}{s\tau K} + u} - cv.$$

Rescaling time by $t = \frac{t^*}{r}$ will prove to be helpful as well. The chain rule gives

$$\frac{df}{dt^*} = \frac{df}{dt}\frac{dt}{dt^*} = \frac{df}{dt}\frac{1}{r}.$$

Rewriting the system according to this change yields

$$\dot{u} = u(1 - u) - \frac{\frac{d}{r\tau}uv}{\frac{1}{s\tau K} + u},$$
$$\dot{v} = \frac{\frac{d}{r\tau}uv}{\frac{1}{s\tau K} + u} - \frac{c}{r}v,$$

where now the dot on top of the u and v denotes the time derivative w.r.t. t^*. Finally, set $a = \frac{d}{r\tau}$ as well as $b = \frac{1}{s\tau K}$ and $E = \frac{c}{r}$, then the system takes the form

$$\dot{u} = u(1 - u) - \frac{auv}{b + u},$$
$$\dot{v} = \frac{auv}{b + u} - Ev.$$

Observe that this system now only contains three parameters but is equivalent to the initial system. Given that all parameters in the original system were assumed to be strictly positive, it follows that also the new parameters a, b and E are strictly positive as well.

It can be shown that for the system at hand, the first quadrant, which is given by

$$Q = \{(x_1, x_2) \in \mathbb{R}^2 | x_1, x_2 \geq 0\},$$

is positively invariant. Further, solutions with initial conditions in Q are bounded. For a proof of these properties the reader is referred to the article by Smith [10]. The

first quadrant will be assumed to be the phase space throughout this thesis since negative population densities do not make any sense in this ecological setting. The system equations have been simplified by rescaling and we know that solutions with initial conditions in the first quadrant are well defined and stay in the first quadrant. This lays the foundation to be able to investigate equilibria and their stability and assign meaningful interpretations.

2.3 Equilibria and their Stability

Having found that the system can be rescaled to the form

$$\begin{aligned} \dot{x}_1 &= f_1(x_1, x_2) = x_1(1 - x_1) - \frac{a x_1 x_2}{b + x_1}, \\ \dot{x}_2 &= f_2(x_1, x_2) = \frac{a x_1 x_2}{b + x_1} - d x_2, \end{aligned} \tag{2}$$

the equilibria can be found by finding the intersections of the x_1 and x_2-nullclines, that is, locating points (x_1, x_2) for which $\dot{x}_1 = 0$ and $\dot{x}_2 = 0$. The equations

$$\begin{aligned} 0 &= x_1\Big[(1 - x_1) - \frac{a x_2}{b + x_1}\Big], \\ 0 &= x_2\Big[\frac{a x_1}{b + x_1} - d\Big], \end{aligned}$$

are solved for x_1 and x_2 to find the nullclines. From this point forward denote

$$\boldsymbol{x} = \begin{bmatrix} x_1 \\ x_2 \end{bmatrix}.$$

The x_1-nullclines are given by

$$\begin{aligned} N_1 &= \{\boldsymbol{x} \in \mathbb{R}^2 |\ x_1 = 0\}, \\ N_2 &= \{\boldsymbol{x} \in \mathbb{R}^2 |\ x_2 = \frac{1}{a}(1 - x_1)(b + x_1)\}, \end{aligned}$$

and the x_2-nullclines by

$$\begin{aligned} N_3 &= \{\boldsymbol{x} \in \mathbb{R}^2 |\ x_2 = 0\}, \\ N_4 &= \{\boldsymbol{x} \in \mathbb{R}^2 |\ x_1 = \frac{bd}{a - d}\}. \end{aligned}$$

To get some geometric intuition for the location and behaviour of the nullclines, figure 1 illustrates the nullclines for two different parameter settings.

The only equilibria which are of importance in this case, are the ones which are located in the first quadrant. From the equations of the nullclines and by inspection of figure 1, it follows that there are at least 2 and at most 3 equilibria in the first quadrant. The points $(0, 0)$ and $(1, 0)$ are always equilibria of the system, independent of the parameter configuration. The third and by far the most interesting equilibrium is the intersection of the non-trivial nullclines, namely the intersection of the parabola $x_2 = \frac{1}{a}(1 - x_1)(b + x_1)$ and the vertical line $v = \frac{bd}{a-d}$. This equilibrium $(\bar{x}_1, \bar{x}_2)$ will be called the *coexistence equilibrium*. Since all parameters are assumed to be positive, a

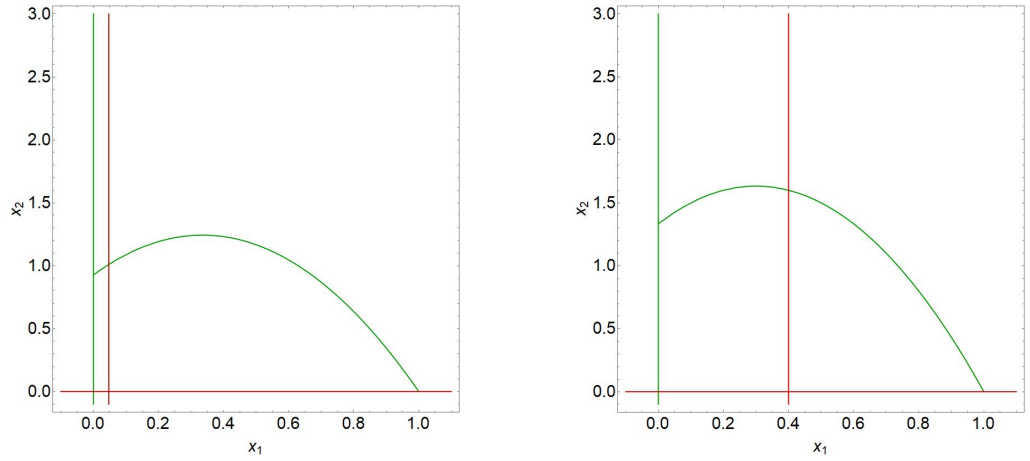

Figure 1: Nullclines for parameters values $a = 0.3556$, $b = 0.33$ and $d = 0.0444$ (left), and $a = 0.3$, $b = 0.4$ and $d = 0.15$ (right). The x_1-nullclines are in green, the x_2-nullclines in red.

necessary and sufficient condition for the occurrence of the coexistence equilibrium in the interior of the first quadrant is given by

$$0 < \frac{bd}{a-d} < 1. \tag{3}$$

The case where the coexistence equilibrium coincides with $(1, 0)$ is excluded. In the following it assumed that inequality (3) holds. Explicitly, the coexistence equilibrium is given by

$$(\bar{x}_1, \bar{x}_2) = \Big(\frac{bd}{a-d}, \frac{b(a-bd-d)}{(a-d)^2}\Big).$$

To investigate the stability of the equilibria located at the origin and $(1, 0)$, it will be sufficient to consider the linearized system around those points. The Jacobian matrix for the system (2) is given by

$$J(x_1, x_2) = \begin{bmatrix} \frac{\partial f_1}{\partial x_1} & \frac{\partial f_1}{\partial x_2} \\ \frac{\partial f_2}{\partial x_1} & \frac{\partial f_2}{\partial x_2} \end{bmatrix} = \begin{bmatrix} 1 - 2x_1 - \frac{abx_2}{(b+x_1)^2} & -\frac{ax_1}{b+x_1} \\ \frac{abx_2}{(b+x_1)^2} & \frac{ax_1}{b+x_1} - d \end{bmatrix}$$

To find the matrices which represent the system equations for the linearized systems around the equilibria, the Jacobian matrix is evaluated at $(0, 0)$ and $(1, 0)$. This yields

$$J(0,0) = \begin{bmatrix} 1 & 0 \\ 0 & -d \end{bmatrix} \qquad \text{and} \qquad J(1,0) = \begin{bmatrix} -1 & -\frac{a}{b+1} \\ 0 & \frac{a}{b+1} - d \end{bmatrix}.$$

The eigenvalues of $J(0, 0)$ are 1 and $-d$. Since $d > 0$, this implies that the origin is a saddle point of system (2). Similarly so for $J(1, 0)$; the eigenvalues are -1 and

$$\frac{a}{b+1} - d = \frac{(a-d) - bd}{b+1} > 0,$$

as can be seen when invoking inequality (3). It follows that $(1, 0)$ is a saddle point as well. Investigating the stability of the coexistence equilibrium is a more delicate matter. In this case the stability actually depends on the parameter configuration.

Claim. *The coexistence equilibrium* $(\bar{x}_1, \bar{x}_2)$ *is a source if* $b < \frac{a-d}{a+d}$ *and a sink if* $b > \frac{a-d}{a+d}$.

Proof. Note that the term in the second row and second column of $J(\bar{x}_1, \bar{x}_2)$ gives zero:

$$\frac{a\bar{v}}{b+\bar{x}_1} - d = \frac{a\frac{bd}{a-d}}{b+\frac{bd}{a-d}} - d = 0$$

Even though the explicit computation of eigenvalues of $J(\bar{x}_1, \bar{x}_2)$ is possible, another way to reason about the stability of $(\bar{x}_1, \bar{x}_2)$ is to note that

$$det(J(\bar{x}_1, \bar{x}_2)) = det \begin{bmatrix} 1 - 2\bar{x}_1 - \frac{ab\bar{x}_2}{(b+\bar{x}_1)^2} & -\frac{a\bar{x}_1}{b+\bar{x}_1} \\ \frac{ab\bar{x}_2}{(b+\bar{x}_1)^2} & 0 \end{bmatrix} = \frac{a^2 b\bar{x}_1\bar{x}_2}{(b+\bar{x}_1)^3} > 0$$

A standard result from linear algebra states that the determinant of a matrix is equal to the product of the eigenvalues. Since the determinant of $J(\bar{x}_1, \bar{x}_2)$ is positive, this means that the eigenvalues could be both positive, both negative or nonzero complex conjugates. Further, the trace of a matrix is equal to the sum of the eigenvalues. The equation for the nontrivial x_1-nullcline,

$$x_2 = \frac{1}{a}(1 - x_1)(b + x_1),$$

relates $\bar{x}_1$ and $\bar{x}_2$ in a convenient way. Substituting for $\bar{x}_2$, the trace of the Jacobian matrix is given by

$$\begin{aligned} tr(J(\bar{x}_1, \bar{x}_2)) &= 1 - 2\bar{x}_1 - \frac{ab\bar{x}_2}{(b+\bar{x}_1)^2} \\ &= 1 - 2\bar{x}_1 - \frac{ab}{(b+\bar{x}_1)^2}\big[\frac{1}{a}(1-\bar{x}_1)(b+\bar{x}_1)\big] \\ &= \frac{\bar{x}_1(1-b-2\bar{x}_1)}{b+\bar{x}_1}. \end{aligned}$$

Both b and $\bar{x}_1$ are positive and thus the sign of the trace only depends on the term $1-b-2\bar{x}_1$. In the case that both eigenvalues λ_1 and λ_2 are real numbers, this means that both λ_1 and λ_2 have the same sign as the term $1-b-2\bar{x}_1$. On the other hand, if the eigenvalues are complex conjugates, then

$$2Re(\lambda_1) = 2Re(\lambda_2) = \lambda_1 + \lambda_2 = tr(J(\bar{x}_1, \bar{x}_2))$$

and hence the signs of $Re(\lambda_1)$ and $Re(\lambda_2)$ are the same and equal to the sign of $1-b-2\bar{x}_1$. It follows that the coexistence equilibrium $(\bar{x}_1, \bar{x}_2)$ is a source if $1-b-2\bar{x}_1 > 0$ and a sink if $1-b-2\bar{x}_1 < 0$. Substituting $\bar{x}_1 = \frac{bd}{a-d}$ and rewriting yields the wanted result. □

Geometrically this means that the coexistence equilibrium is a source if $\bar{x}_1$ lies to the left of the maximum of the parabola $x_2 = \frac{1}{a}(1-x_1)(b+x_1)$ while it is a sink if it lies to the right of the maximum. For a more detailed discussion of the relationship between the stability behaviour of a planar linear system and the trace-determinant plane of the corresponding system matrix, the reader is referred to appendix A.

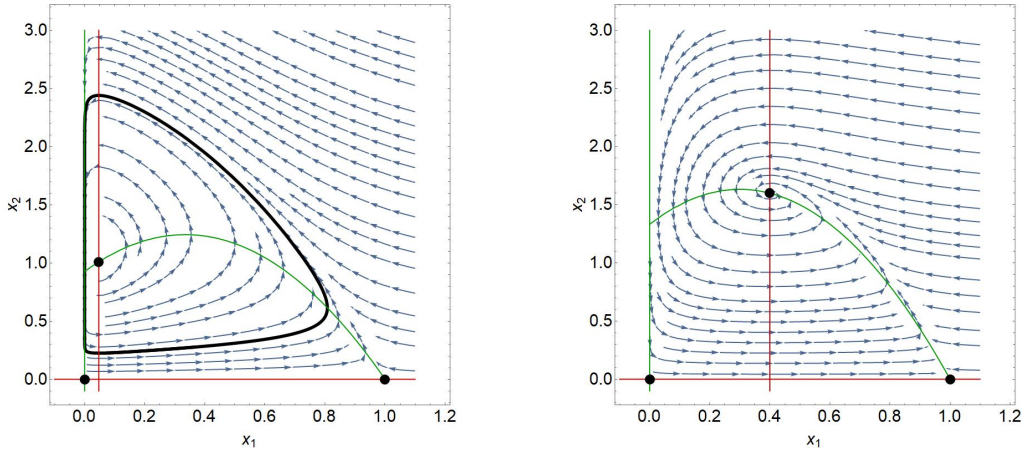

Figure 2: Phase portraits for $a = 0.4$, $b = 0.3$ and $d = 0.1$ (left), and $a = 0.3$, $b = 0.4$ and $d = 0.15$ (right).

The phase portraits together with nullclines, equilibria and periodic solutions for two different parameter settings are shown in figure 2. The vector field is indicated by blue arrows, the nullclines are green and red as before. Equilibria are illustrated by black dots and periodic orbits as thick black lines.

The preceding discussion might lead one to expect that there exists a Hopf bifurcation for $b = \frac{a-d}{a+d}$ and this is indeed the case. The following claim summarizes this speculation.

Claim. *There exists a periodic solution for* $b < \frac{a-d}{a+d}$ *which vanishes in a Hopf bifurcation for* $b = \frac{a-d}{a+d}$.

A proof for this claim can be found in the article by Smith [10].

In this chapter the most important features of the dynamics of the Rosenzweig-MacArthur model have been outlined. The system equations were derived from biological principles and then rescaled. Nullclines, equilibria and periodic solutions to the rescaled systems have been examined. The existence of a Hopf bifurcation under the variation of the parameters (b in particular) has been established. Now that the predator-prey model is understood in its continuous form, we shall turn to the analysis of the modified model including a harvesting effort which depends on the abundance of the predators. In doing so, it is necessary to familiarize the reader with some basic notions of planar piecewise-smooth dynamical systems.

3 Filippov Systems

In this chapter, the notion of a planar Filippov system will be introduced. Definitions and results presented in this chapter are taken from the articles by Kuznetsov et. al. [8] and the PhD thesis by X. Liu [9]. Filippov systems are piecewise-smooth dynamical systems. That means they are dynamical systems for which the phase space is partitioned into multiple regions $S_i \subset \mathbb{R}^n$ where $i = 1, ..., k$. Any two regions S_i and S_j are separated by a set $\Sigma_{i,j}$ and on each region S_i the governing flow is given by

$$\dot{\boldsymbol{x}} = F_i(\boldsymbol{x}),\ \boldsymbol{x} \in S_i,\ i = 1, ..., k,$$

Where each F_i is a smooth vector field. Treating Filippov systems of arbitrary dimension definitely has its attractiveness but given that the aim of this thesis is to investigate predator-prey interactions for a two-dimensional model, it will suffice to treat planar systems.

As should be clear from the preceding introduction to Filippov systems of arbitrary dimension, the flow on each region S_i is well defined and smooth. However, there is nothing stated about what happens once a solutions reaches a discontinuity boundary $\Sigma_{i,j}$. To answer this question for the planar case, Filippov's convex method will be introduced. This will yield a new system of equations describing how solutions behave on the discontinuity boundary. The next step is then to classify equilibria to the newly defined system on the boundary. Uniqueness of solutions in Filippov systems will briefly be examined and the notion of topological equivalence will be introduced. Finally, definitions for local and global discontinuity-induced bifurcations (DIBs) will be derived from the notion of topological equivalence.

3.1 Planar Filippov Systems

In general, a Filippov system on $\mathbb{R}^2$ can have any number of discontinuity boundaries. However, in order to understand the essential mechanisms at any of those boundaries, it suffices to investigate a simple system consisting of only two regions S_1 and S_2, with smooth vector fields $f^{(1)}(\boldsymbol{x})$ and $f^{(2)}(\boldsymbol{x})$ defined on them:

$$\dot{\boldsymbol{x}} = \begin{cases} f^{(1)}(\boldsymbol{x}), & \boldsymbol{x} \in S_1, \\ f^{(2)}(\boldsymbol{x}), & \boldsymbol{x} \in S_2. \end{cases} \tag{4}$$

The regions S_1 and S_2, as well as the boundary Σ separating them, are similarly defined by

$$\begin{aligned} S_1 &= \{\boldsymbol{x} \in \mathbb{R}^2 : H(\boldsymbol{x}) < 0\}, \\ S_2 &= \{\boldsymbol{x} \in \mathbb{R}^2 : H(\boldsymbol{x}) > 0\}, \\ \Sigma &= \{\boldsymbol{x} \in \mathbb{R}^2 : H(\boldsymbol{x}) = 0\}. \end{aligned}$$

Here, H is a smooth function, mapping from $\mathbb{R}^2$ to $\mathbb{R}$, with the property that its gradient does not vanish anywhere on Σ. It follows that $\nabla H(\boldsymbol{x})$ is perpendicular to Σ at every point. The discontinuity boundary Σ is either a closed loop or it extends to infinity in both directions. Moreover, $f^{(1)}$ and $f^{(2)}$ are not identical on Σ. This justifies the name "discontinuity boundary". Note that, if restricted to S_1 or S_2,

system (4) defines a smooth, planar dynamical system, which is well studied. Finally, observe that by virtue of the definitions made above, the following holds:

$$\mathbb{R}^2 = S_1 \cup \Sigma \cup S_2$$

On both S_1 and S_2 the dynamics are well known, but what happens when a solution curve reaches Σ? This question will be answered in the following discussion of what is today known as Filippov's convex method.

3.2 Filippov's Convex Method

In his book, *Differential Equations with Discontinuous Righthand Sides* [5], A.F. Filippov explores the question of how to define differential equations that govern the behaviour of piecewise-smooth dynamical systems on discontinuity boundaries. He found that two different things can happen when a solution reaches Σ: The solution either *crosses* Σ and continues its path as dictated by the vector field of the region it crossed over to, or it stays on Σ. The behaviour of a solution that stays on Σ is called *sliding*. To describe these solutions, Σ is split up into a region where sliding can occur and another region where sliding cannot occur. To make the notion more rigorous, σ will function as an indicator and we define it as

$$\sigma(\boldsymbol{x}) = \langle \nabla H(\boldsymbol{x}), f^{(1)}(\boldsymbol{x}) \rangle \langle \nabla H(\boldsymbol{x}), f^{(2)}(\boldsymbol{x}) \rangle,$$

where $\langle \cdot, \cdot \rangle$ denotes the standard inner product on $\mathbb{R}^2$.

Definition. *The set* $\Sigma_c = \{\boldsymbol{x} \in \Sigma : \sigma(\boldsymbol{x}) > 0\}$ *is called the* ***crossing set*** *and the set* $\Sigma_s = \{\boldsymbol{x} \in \Sigma : \sigma(\boldsymbol{x}) \leq 0\}$ *is called the* ***sliding set****.*

It is worth pointing out that Σ_c is open while Σ_s consists of the union of closed *sliding segments* and *isolated sliding points*, hence Σ_s is closed.

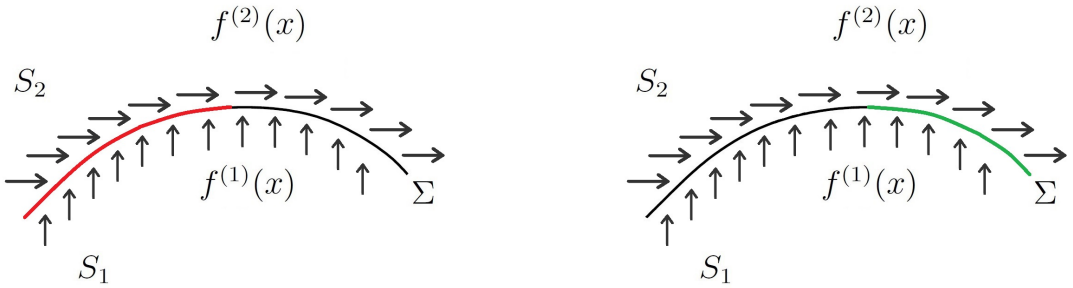

Figure 3: Examples of segments in a sliding set (left) and crossing set (right). The sliding segment is highlighted in red, the crossing segment in green. Note that sliding motion is also possible when the vectors point away from Σ.

To give some geometric intuition about the crossing and sliding sets, consider a point $\boldsymbol{x}$ in the crossing set Σ_c. By definition $\sigma(\boldsymbol{x}) > 0$. This means that both $\langle \nabla H, f^{(1)} \rangle$ and $\langle \nabla H, f^{(2)} \rangle$ are nonzero and have the same sign, which in turn means that both $f^{(1)}(\boldsymbol{x})$ and $f^{(2)}(\boldsymbol{x})$ have nonzero normal components pointing in the same direction (normal w.r.t. Σ). Hence, if a solution in S_1 or S_2 reaches a point $\boldsymbol{x} \in \Sigma_c$, it would be natural to define the solution in such a way that it *crosses* Σ. An example of segments within the crossing and sliding set is illustrated in figure 3.

On the other hand, consider a point $\boldsymbol{x}$ in the sliding set Σ_s. By definition $\sigma(\boldsymbol{x}) \leq 0$. This can mean different things. One possibility is that $\langle \nabla H, f^{(1)} \rangle$ or $\langle \nabla H, f^{(2)} \rangle$ vanish. Another possibility is that $\langle \nabla H, f^{(1)} \rangle$ and $\langle \nabla H, f^{(2)} \rangle$ are nonzero but have opposite signs at x. Geometrically this indicates that either,

a) $f^{(1)}(\boldsymbol{x})$ or $f^{(2)}(\boldsymbol{x})$ have zero normal components,

b) both have nonzero normal components pointing either towards or away from Σ.

In either case, if a solution reaches a point $\boldsymbol{x} \in \Sigma_s$, then it seems natural to expect the solution to stay on Σ, however, on Σ there is no governing equation defined. To be able to meaningfully define a vector field on Σ_s, one more definition needs to be made, namely the one for *singular sliding points*.

Definition. *Points $\boldsymbol{x}$ in the sliding set Σ_s such that $\langle \nabla H(\boldsymbol{x}), f^{(2)}(\boldsymbol{x}) - f^{(1)}(\boldsymbol{x}) \rangle = 0$ are called* ***singular sliding points****.*

Why this definition is needed will become evident on the next page. At a singular sliding point the following holds:

$$\langle \nabla H(\boldsymbol{x}), f^{(1)}(\boldsymbol{x}) \rangle = \langle \nabla H(\boldsymbol{x}), f^{(2)}(\boldsymbol{x}) \rangle = 0.$$

This follows from the fact that for points in the sliding set $\sigma(\boldsymbol{x}) \leq 0$ and by the definition of a singular sliding point. At these points both $f^{(1)}(\boldsymbol{x})$ and $f^{(2)}(\boldsymbol{x})$ are zero, or one of them is zero while the other is tangent to Σ, or both $f^{(1)}(\boldsymbol{x})$ and $f^{(2)}(\boldsymbol{x})$ are tangent to Σ. As we will see now, these are points that have to be treated with special care.

The Convex Method

In order to define a vector field on Σ_s, Filippov proposed to set the right-hand side of the differential equation equal to the unique linear convex combination of $f^{(1)}(\boldsymbol{x})$ and $f^{(2)}(\boldsymbol{x})$ that is tangent to Σ_s at a point $\boldsymbol{x}$. This is illustrated in figure 4.

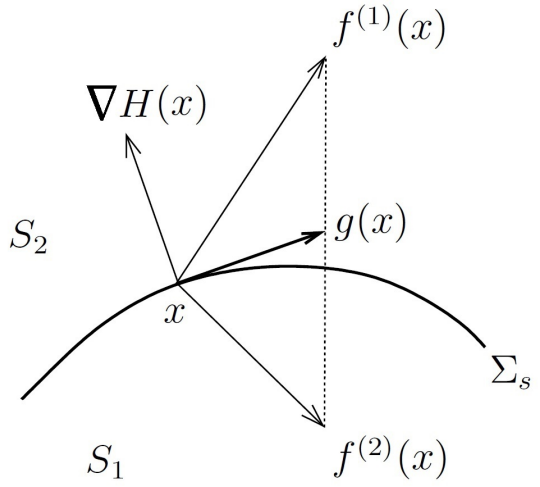

Figure 4: Filippov's convex method. Source: Kuznetsov et al. [8]

The mathematical description of g (and λ) is given by

$$g(\boldsymbol{x}) = \lambda f^{(1)}(\boldsymbol{x}) + (1 - \lambda) f^{(2)}(\boldsymbol{x}),$$

$$\lambda = \frac{\langle \nabla H(\boldsymbol{x}), f^{(2)}(\boldsymbol{x}) \rangle}{\langle \nabla H(\boldsymbol{x}), f^{(2)}(\boldsymbol{x}) - f^{(1)}(\boldsymbol{x}) \rangle}.$$

Note that this construction only makes sense when talking about non-singular sliding points, as otherwise the denominator in the expression for λ becomes zero. This motivated the definition of singular sliding points in the first place. It can easily be shown that the vector $g(\boldsymbol{x})$ is tangent to Σ_s for all non-isolated sliding points in Σ_s. Suppose $\boldsymbol{x} \in \Sigma_s$ is a non-isolated sliding point, then

$$\begin{aligned}
\langle \nabla H(\boldsymbol{x}), g(\boldsymbol{x}) \rangle &= \langle \nabla H(\boldsymbol{x}), \lambda f^{(1)}(\boldsymbol{x}) + (1-\lambda) f^{(2)}(\boldsymbol{x}) \rangle \\
&= \lambda \langle \nabla H(\boldsymbol{x}), f^{(1)}(\boldsymbol{x}) \rangle + (1-\lambda) \langle \nabla H(\boldsymbol{x}), f^{(2)}(\boldsymbol{x}) \rangle \\
&= \frac{1}{\eta} \Big[\langle \nabla H(\boldsymbol{x}), f^{(2)}(\boldsymbol{x}) \rangle \langle \nabla H(\boldsymbol{x}), f^{(1)}(\boldsymbol{x}) \rangle \\
&+ \quad \langle \nabla H(\boldsymbol{x}), f^{(2)}(\boldsymbol{x}) - f^{(1)}(\boldsymbol{x}) \rangle \langle \nabla H(\boldsymbol{x}), f^{(2)}(\boldsymbol{x}) \rangle \\
&- \quad \langle \nabla H(\boldsymbol{x}), f^{(2)}(\boldsymbol{x}) \rangle \langle \nabla H(\boldsymbol{x}), f^{(2)}(\boldsymbol{x}) \rangle \Big] \\
&= 0,
\end{aligned}$$

where η is a placeholder term defined as

$$\eta = \langle \nabla H(\boldsymbol{x}), f^{(2)}(\boldsymbol{x}) - f^{(1)}(\boldsymbol{x}) \rangle.$$

So indeed $g(\boldsymbol{x})$ is tangent to Σ_s for all non-isolated sliding points $\boldsymbol{x} \in \Sigma_s$, or put differently, $g(\boldsymbol{x})$ is always tangent to sliding segments.

For non-isolated singular sliding points which are not infinitely-degenerate, $g(\boldsymbol{x})$ and its derivatives are defined by continuity. At isolated singular sliding points $g(\boldsymbol{x})$ is set to be zero. Having carefully defined what $g(\boldsymbol{x})$ should be for the different types of points on Σ_s, it is now possible to define a differential equation on Σ_s:

$$\dot{\boldsymbol{x}} = g(\boldsymbol{x}),\ \boldsymbol{x} \in \Sigma_s \tag{5}$$

As a result of meticulously treating the different points on Σ_s, the sliding system (5) is smooth on sliding segments of Σ_s.

Definition. *Solutions to equation (5) are called* ***sliding solutions****.*

Having finally arrived at an equation that describes what happens on the sliding set, a natural next step is to investigate the equilibria of the sliding system.

3.3 The Sliding System and Equilibria

The sliding system (5) is a dynamical system in its own right and equilibria are a good place to start when examining such systems. All isolated singular sliding points are equilibrium points of the sliding system, as $g(\boldsymbol{x})$ is *set* to be zero there. There are two types of equilibria to be considered, namely pseudo-equilibria and boundary equilibria.

Definition.

(i) An equilibrium $\bar{\boldsymbol{x}} \in \Sigma_s$ of system (2) is called a ***pseudo-equilibrium*** *if $f^{(1)}(\bar{\boldsymbol{x}})$ and $f^{(2)}(\bar{\boldsymbol{x}})$ are anti-collinear and transversal to Σ_s.*

(ii) An equilibrium $\bar{\boldsymbol{x}} \in \Sigma_s$ of system (2) is called a ***boundary equilibrium*** *if $f^{(1)}(\bar{\boldsymbol{x}})$ or $f^{(2)}(\bar{\boldsymbol{x}})$ is zero.*

Another special type of point on the discontinuity boundary which will be of great importance are the so called tangent points.

Definition. *A point $\boldsymbol{T}$ is called a* ***tangent point*** *if both $f^{(1)}(\boldsymbol{T})$ and $f^{(2)}(\boldsymbol{T})$ are non-zero but one of them is tangent to Σ.*

A direct consequence of the definitions above is that pseudo-equilibria can only occur within sliding segments, i.e. they never mark the endpoint of a sliding segment. Sliding segments are delimited either by a boundary equilibrium or by a tangent point. The fact that only generic Filippov systems are under consideration eliminates the possibility of accumulation of equilibria and tangent points. Further, boundary equilibria can be interpreted as regular equilibria of the systems defined on S_1 and S_2 that happen to occur on the discontinuity boundary Σ. Knowing how solutions behave on the discontinuity boundary and also what kinds of equilibria occur on Σ_s, it is now time to make more precise what is meant by a solution of a Filippov system.

3.4 Solutions of Filippov systems

As already discussed in section 3.2, solutions that reach the discontinuity boundary Σ either cross or slide on the boundary. In the following, the notion of a "solution" will be made more precise. The stated assumptions can be made without loss of generality when one considers the renaming of the regions and vector fields.

Assume $\boldsymbol{x}(t)$, $t \in \mathbb{R}$, is a solution to the smooth dynamical system

$$\begin{aligned} \dot{\boldsymbol{x}} &= f^{(1)}(\boldsymbol{x}), \\ \boldsymbol{x}(0) &= \boldsymbol{x}_0 \in S_1. \end{aligned}$$

Now suppose $\boldsymbol{x}(t)$ reaches Σ for some time $t = t_1 > 0$. More formally this means that $H(\boldsymbol{x}(t_1)) = 0$. Two things can happen:

Case 1: The point of interest $\boldsymbol{x}(t_1)$ lies in Σ_c and we set

$$\dot{\boldsymbol{x}} = f^{(2)}(\boldsymbol{x}) \text{ for } t \geq t_1,$$

that is, the solution crosses Σ and is continued as dictated by the flow on S_2.

Case 2: The point of interest $\boldsymbol{x}(t_1)$ lies in Σ_s and we set

$$\dot{\boldsymbol{x}} = g(\boldsymbol{x}) \text{ for } t \geq t_1. \tag{6}$$

If $g(\boldsymbol{x}(t_1)) = 0$, then set $\boldsymbol{x}(t) = \boldsymbol{x}(t_1)$ for all $t > t_1$. If $g(\boldsymbol{x}(t_1)) \neq 0$, then we solve system (6). This solution can stay strictly within the sliding segment forever as it approaches a pseudo-equilibrium or a singular sliding point. Other possibilities are that the solution reaches a boundary equilibrium or a tangent point at some time $t_2 > t_1$. If it reaches a boundary equilibrium set $\boldsymbol{x}(t) = \boldsymbol{x}(t_2)$ for all $t > t_2$. If it reaches a tangent point then set

$$\dot{\boldsymbol{x}} = f^{(1)}(\boldsymbol{x}) \text{ or } \dot{\boldsymbol{x}} = f^{(2)}(\boldsymbol{x}), \text{ for } t > t_2,$$

depending on which flow is tangent to Σ at $\boldsymbol{x}(t_2)$.

Note that this notion of a unique forward solution is conform with the existence and uniqueness theorem (Picard-Lindelöf). This is because the function describing the right-hand side of the differential equation is uniformly Lipschitz continuous on both regions and hence whenever a solution crosses from one region into another or starts sliding on Σ_s, the corresponding Lipschitz constant can be taken to be the greater one of the two constants in question.

The consideration of Case 1 and Case 2 as above defines a unique forward solution to the system (4) and hence to the entire Filippov system. The same reasoning can be applied to construct a unique backward solution by considering

$$f^{(i)}(\boldsymbol{x}) \mapsto -f^{(i)}(\boldsymbol{x}).$$

It is to be pointed out that since orbits can overlap, system (4) is not invertible in the classical sense, i.e. orbits passing through some point $\boldsymbol{x}_0$ in the phase space need not be uniquely determined. Equipped with these notions of unique forward and backward solutions we can now classify tangent points into two classes, visible and invisible tangent points.

Definition. *A tangent point $\boldsymbol{T}$ is called **visible** if the orbit of $\dot{\boldsymbol{x}} = f^{(i)}(\boldsymbol{x})$, starting at $\boldsymbol{T}$, stays in S_i for sufficiently small $|t| \neq 0$. Similarly, a tangent point $\boldsymbol{T}$ is called **invisible** if the orbit to $\dot{\boldsymbol{x}} = f^{(i)}(\boldsymbol{x})$, starting at $\boldsymbol{T}$, does not belong to S_i for sufficiently small $|t| \neq 0$.*

The the illustration in figure 5 depicts both situations. Note that the notion of visibility of a tangent point is tied to a specific region this refers to. It is very well possible for a tangent point to be a visible tangent point to some region and at the same time being an invisible tangent point to a different region. These kinds of double tangencies do not occur in the modified Rosenzweig-Macarthur model under consideration and will hence no further be studied.

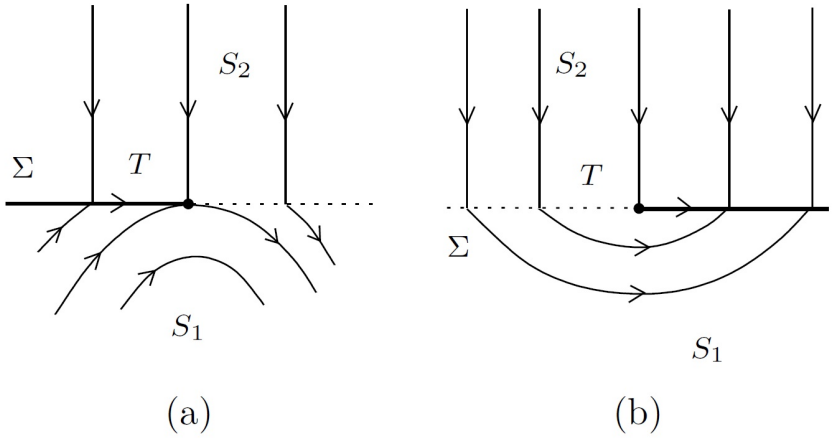

Figure 5: Generic visible (a) and invisible (b) tangent points. Source: Kuznetsov et al.[8].

We call a tangent point $\boldsymbol{T}$, where $f^{(i)}$ is tangent to Σ, *quadratic* if the orbit through $\boldsymbol{T}$ can be locally represented by

$$x_j = \frac{1}{2}\mu x_i^2 + O(x_i^3),\ \mu \neq 0.$$

with $i, j \in \{1, 2\}$ and $i \neq j$.

All the definitions made so far are going to be of critical importance when examining discontinuity-induced bifurcations. In the following discussion of topological equivalence for Filippov Systems, the notion of bifurcation will be introduced. When proposing criteria for both local and global bifurcations it will become clearer how all the discussed theory interconnects.

3.5 Topological Equivalence and Bifurcations

A dynamical system is said to undergo a bifurcation if upon smooth variation of a system parameter, the behaviour of that system changes qualitatively. The notion of topological equivalence is a powerful tool in making this notion of a "qualitative change of behaviour" more precise.

Definition. *Two Filippov systems are called* ***topologically equivalent*** *if there exists a homeomorphism $h : \mathbb{R}^2 \to \mathbb{R}^2$, which maps the phase portrait of one system onto the one of the other, while preserving orientation of the solutions.*

The phase portrait to a system (4) is the union of all its orbits and the term orbit is here to be understood with respect to the unique forward and backward solutions as defined earlier. Now suppose two systems A and B are topologically equivalent. This means that if $O_1 = \{\boldsymbol{x}(t)\}$ is an arbitrary orbit of system A, then $O_2 = \{h(\boldsymbol{x}(t))\}$ is an orbit of system B. The same holds the other way around with h^{-1} respectively. If such a homeomorphism between two systems exists, then sliding segments of one system get mapped onto the sliding segments of the other and vice versa. Further, it is natural to require that the function h maps the discontinuity boundary Σ of one system onto the discontinuity boundary Σ' of the other system.

Recalling the form of the initial system (4), the next step is to define a planar Filippov system which depends on a single parameter α. Consider the following system equation,

$$\dot{\boldsymbol{x}} = \begin{cases} f^{(1)}(\boldsymbol{x}, \alpha), & \boldsymbol{x} \in S_1(\alpha), \\ f^{(2)}(\boldsymbol{x}, \alpha), & \boldsymbol{x} \in S_2(\alpha), \end{cases} \quad \boldsymbol{x} \in \mathbb{R}^2 \text{ and } \alpha \in \mathbb{R}. \tag{7}$$

Now S_1, S_2 and Σ are defined by

$$\begin{aligned} S_1(\alpha) &= \{\boldsymbol{x} \in \mathbb{R}^2 : H(\boldsymbol{x}, \alpha) < 0\}, \\ S_2(\alpha) &= \{\boldsymbol{x} \in \mathbb{R}^2 : H(\boldsymbol{x}, \alpha) > 0\}, \\ \Sigma(\alpha) &= \{\boldsymbol{x} \in \mathbb{R}^2 : H(\boldsymbol{x}, \alpha) = 0\}, \end{aligned}$$

where, $H(\boldsymbol{x}, \alpha)$ is again a smooth function such that $\nabla_{\boldsymbol{x}} H(\boldsymbol{x}, \alpha) \neq 0$ for all $\boldsymbol{x} \in \mathbb{R}^2$ and $\alpha \in \mathbb{R}$. Note that α is a parameter and $\nabla_{\boldsymbol{x}}$ denotes the gradient with respect to the variables in phase space. Further, $f^{(1)}$ and $f^{(2)}$ are smooth functions of both $\boldsymbol{x}$ and α.

Definition. *We say that system (7) displays a* ***bifurcation*** *for some parameter value $\alpha = \alpha_0$, if by an arbitrarily small parameter perturbation from α_0, the system changes in such a way that the systems, before and after the perturbation, are not topologically equivalent.*

There are two types of bifurcations to be considered; *local* and *global* bifurcations.

Definition. *A bifurcation is considered to be* ***local*** *if the change of behavior can be observed in an arbitrarily small fixed neighborhood of a point $x \in \mathbb{R}^2$. A bifurcation is said to be* ***global*** *if it is not local.*

An example of a local bifurcation is the collision of an equilibrium with the discontinuity boundary. An example of a global bifurcation is the collision of a limit cycle with the discontinuity boundary. The appearance/disappearance of a sliding segment is already a bifurcations as phase portraits with overlapping orbits cannot be homeomorphic to phase portraits without overlapping.

Bifurcation criteria

To be able to say something about local and global bifurcations in the modified Rosenzweig-MacArthur model, it is necessary to describe conditions that simplify the detection of bifurcations. In the following derivation of bifurcation criteria, only discontinuity-induced bifurcations will be considered. Local bifurcations are in general easier to detect. To do so it is sufficient to track the location of regular equilibria, equilibria on Σ_s and tangent points. Collisions of these special points mark local bifurcations. The description of conditions for global bifurcations is a bit more delicate and requires a more inventive approach. For the detection of global bifurcations, so called *special orbits* are in focus. A special orbit is an orbit of a Filippov system that re-enters $\mathbb{R}^2 \backslash \Sigma$ from a tangent point or a pseudo-equilibrium. For a bounded special orbit, two cases are to be considered:

1. The special orbit returns to the sliding segment in finite time. The exact location of re-entrance to the sliding segment depends on α. Points of re-entrance can collide with pseudo-equilibria or tangent points. These collisions are considered global bifurcations.

2. The special orbit tends asymptotically to its ω-limit set, which in this case is either a standard stable equilibrium or a stable closed orbit. Collisions of equilibria with Σ are already covered by the discussion of local bifurcations. The collision of a periodic cycle with Σ_s is a global bifurcation.

Another event to be considered a global bifurcation is the appearance of a special orbit that coincides with the separatrix of a standard saddle in S_1 or S_2. An advantage of defining bifurcation criteria as indicated above, is that global bifurcations for which the orbits cross Σ repeatedly but do not slide, are excluded since these cases are qualitatively identical to their smooth analogues.

In this section the reader was introduced to the more theoretical aspects of Filippov systems. In particular equilibria and tangent points on sliding segments in the sliding set Σ_s, as well as bifurcation criteria for planar Filippov systems have been subject of investigation. The following chapter will take the reader on a journey to investigate a selection of the various local and global bifurcations that can be observed in planar Filippov systems.

4 Bifurcation Analysis

In this chapter, a selection of discontinuity-induced bifurcations (DIBs) will be presented. As was discussed in the previous chapter, these are bifurcations that occur in Filippov systems, which are due to interactions with sliding segments of the sliding set Σ_s. In their article, Kuznetsov et al. [8] classify *all* co-dimension one DIBs that occur in generic planar Filippov systems. However, not all co-dimension one DIBs can be observed in the modified Rosenzweig-Macarthur system. In an *a posteriori* approach, this chapter will only deal with DIBs that are relevant for the following discussion of the modified Rosenzweig-Macarthur model. For a comprehensive discussion of all DIBs in generic planar Filippov systems, the reader is referred to article [8].

4.1 Local Bifurcations

In this discussion of local DIBs, the type of local bifurcation will be discussed first and then a *topological normal form* will be introduced. The topological normal form will be a polynomial Filippov system such that every generic Filippov system satisfying the same bifurcation classification criteria is locally topologically equivalent to the normal form. There are three kinds of local bifurcations that occur in the model. These are the so called *boundary focus bifurcation*, the *boundary node bifurcation* and the *pseudo-saddle-node bifurcation*. In order to simplify the classification of bifurcations a few assumptions are made. Without loss of generality it can be assumed that

i) X_α is a hyperbolic equilibrium of system (7) which exists in S_1 for $\alpha < 0$ and collides with Σ for $\alpha = 0$.

ii) The linearized system around X_α has simple eigenvalues. i.e. their algebraic multiplicity is equal to 1 and X_α collides with Σ with a non-zero velocity (w.r.t α).

iii) The collision occurs at a point $X_0 \in \Sigma$ where $f^{(2)}(\boldsymbol{x}, \alpha)$ is transversal to Σ.

In a neighborhood of X_0, so for small α, it can be assumed that $f^{(2)}(\boldsymbol{x}, \alpha)$ is not only transversal, but also orthogonal to Σ. The introduction of flow-box coordinates justifies this assumption. For an introduction to the concept of a flow-box and flow-box coordinates, the reader is referred to appendix A. The first bifurcation under consideration is the boundary-focus-bifurcation.

Boundary focus bifurcation

As the name already suggests, the boundary-focus-bifurcation marks the collision of a standard focus with the discontinuity boundary Σ. In what follows, it is assumed that the focus is unstable with counter-clockwise orientation. Other stability and orientation configurations can be derived by reversing the direction of flow and orientation, as well as reflecting the phase portraits with respect to the vertical axis. Five generic cases are to be considered. A common feature of these five cases is that before the collision there exists a visible tangent point close to X_0 and after the collision there exists an invisible tangent point close to the collision point. There are three aspects which distinguish these cases:

i) The position of the focus nullclines relative to the point T_α.

ii) The orientation of solutions in S_2.

iii) The behaviour of orbits re-entering S_1 through visible tangent point.

The five different cases for the boundary-focus-bifurcation shall henceforth be referred to as BF_i, where $i = 1, ..., 5$.

Type BF$_1$: The phase portraits for a system displaying a boundary-focus bifurcation of type BF_1, as the parameter is varied from $\alpha < 0$, through $\alpha = 0$ and then to $\alpha > 0$ is illustrated in figure 6:

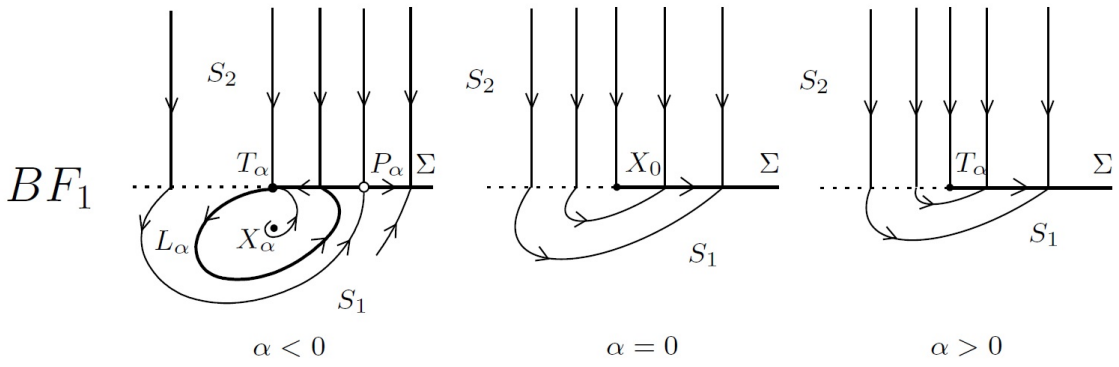

Figure 6: Boundary-focus-bifurcation of type BF_1. Here a stable sliding cycle surrounds the focus for $\alpha < 0$. Source: Kuznetsov et al. [8].

The discontinuity boundary Σ is indicated by a dotted line and sliding segments on Σ are represented by thicker black lines. The notation is to be interpreted as follows. L_α is a stable sliding cycle which surrounds the unstable focus X_α. The point T_α is a visible tangent point delimiting the sliding segment and P_α is a pseudo-saddle. For $\alpha < 0$ the special orbit entering S_1 from T_α returns to the sliding segment between T_α and P_α, hence creating a sliding orbit. At the returning point, both vector fields are transversal to Σ. The basin of attraction for the stable sliding cycle is bounded by the stable separatrices of the pseudo-saddle P_α. As α approaches zero, P_α approaches T_α which in turn approaches X_α as the sliding cycle shrinks. This process ends in the collision of T_α, P_α and X_α, and the disappearance of the sliding cycle for $\alpha = 0$. At $\alpha = 0$, the point of collision X_0 is a boundary equilibrium. For $\alpha > 0$ no more equilibria nor limit cycles exist. The only point of interest on the sliding segment is the invisible tangent point T_α through which a solution arriving from the region S_2 enters the stable sliding segment.

Type BF$_2$: The same situation but now for type BF_2 is illustrated in figure 7. The situation for a bifurcation of type BF_2 is almost identical to the one of BF_1, the only difference is that for $\alpha < 0$ the sliding orbit leaving the segment at T_α returns to the sliding segment to the right of the pseudo-saddle P_α. This means that there is no sliding cycle for $\alpha < 0$. The phase portraits for $\alpha = 0$ and $\alpha > 0$ are identical to the case of BF_1.

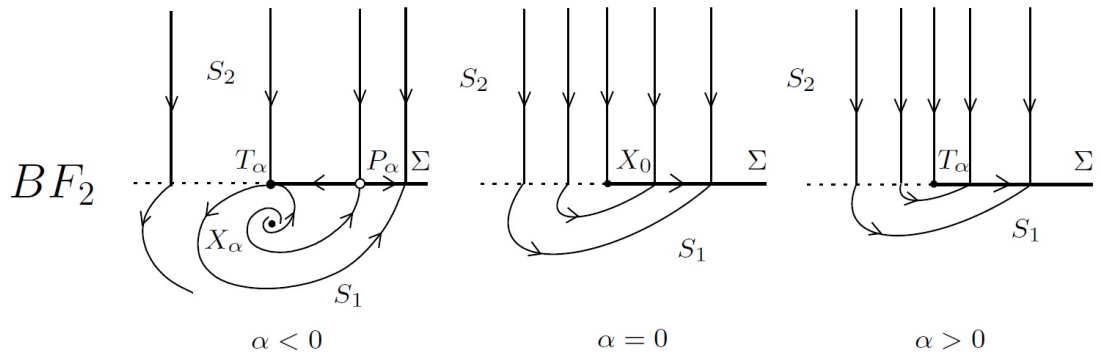

Figure 7: Boundary-focus-bifurcation of type BF_2. Here no stable sliding cycle occurs. Source: Kuznetsov et al. [8]

The types BF_1 are very similar and yet it is possible to analytically tell them apart: Suppose the linearization with respect to the state variables in S_1 around X_0 is given by

$$Jf^{(1)}(X_0, 0) = \begin{bmatrix} a & b \\ c & d \end{bmatrix}.$$

The linearized system is then given by

$$\begin{aligned} \dot{x}_1 &= ax_1 + bx_2, \\ \dot{x}_2 &= cx_1 + dx_2. \end{aligned}$$

Now consider the line $x_2 = 1$ and in particular the orbit passing through the point $T = (-\frac{d}{c}, 1)$. Note that this orbit is tangent to the line $x_2 = 1$ at T and returns to the same line at another point $R = (\theta, 1)$. The type BF_1 corresponds to the case where $\theta < -\frac{b}{a}$ whereas BF_2 corresponds to $\theta > -\frac{b}{a}$. Note that the orbit through T is orthogonal to the line $x_2 = 1$ at R if and only if $\theta = -\frac{b}{a}$. The situation when $\theta = -\frac{b}{a}$ gives rise to a co-dimension 2 bifurcation which Kuznetsov et al. refer to as *degenerate boundary focus* [8]. Since this thesis is primarily concerned with co-dimension one bifurcations, the degenerate boundary focus shall no further be discussed.

Type BF$_3$: The same situation but now for type BF_3 is shown in figure 8.

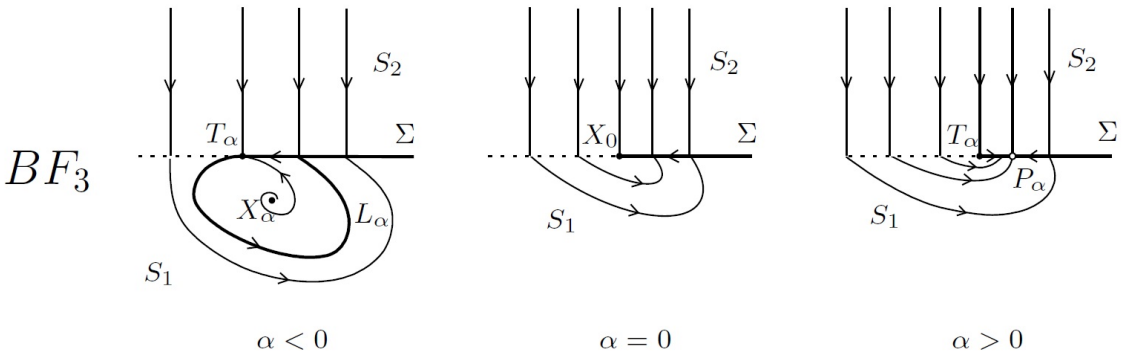

Figure 8: Boundary-focus-bifurcation of type BF_3 and the disappearance of a sliding cycle. Source: Kuznetsov et al. [8].

Similarly to type BF_1, for $\alpha < 0$ there exists a stable sliding cycle L_α which surrounds the unstable focus X_α. The special orbit re-entering S_1 from the tangent point T_α returns to the sliding segment and back to T_α. In contrast to type BF_1, this behaviour is not due to a nearby pseudo-saddle but in this case rather to the position of the focus X_α relative to T_α. As α approaches 0, the sliding orbit shrinks and the point X_α and T_α approach each other. For $\alpha = 0$ the focus and tangent point collide while the sliding cycle completely vanishes. After this collision, for small $\alpha > 0$, all solutions tend to the stable pseudo-equilibrium P_α, which emerged from the collision.

Type BF_4: The phase portraits for a system displaying a boundary-focus bifurcation of type BF_4, as the parameter is varied from $\alpha < 0$, through $\alpha = 0$ and then to $\alpha > 0$ is illustrated in figure 9.

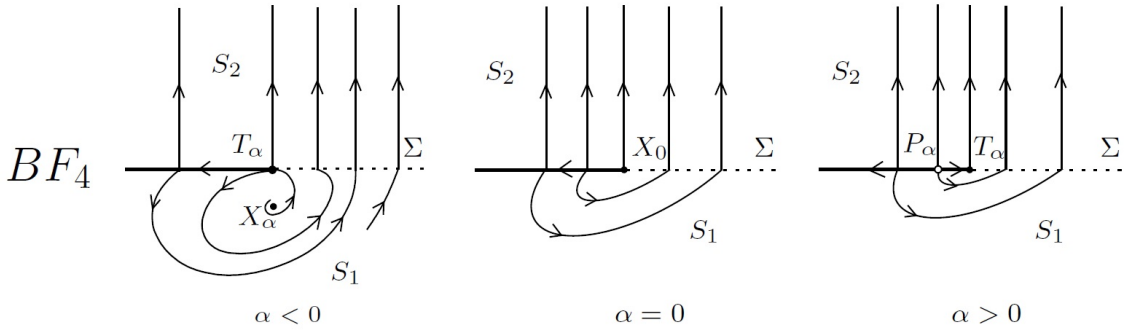

Figure 9: Boundary-focus-bifurcation of type BF_4. Similarly to BF_2, no stable sliding cycle occurs. Source: Kuznetsov et al. [8].

The type BF_4 is very similar to type BF_2. The main difference is that the direction of the vector field $f^{(2)}(\boldsymbol{x})$ has been reversed and hence the sliding segment extends to the left and is unstable. The sliding segment is delimited by the visible tangent point T_α. For $\alpha = 0$ the points X_α and T_α collide and an unstable pseudo-equilibrium emerges from the collision for small $\alpha > 0$. All solution, which are sufficiently close to the focus so that they fall within the neighborhood of our consideration will leave this neighborhood eventually as all occurring equilibira and pseudo-equilibria are unstable and no stable cycle exists near X_α.

Type BF_5: The phase portraits for a system displaying a boundary-focus bifurcation of type BF_5, as the parameter is varied from $\alpha < 0$, through $\alpha = 0$ and then to $\alpha > 0$ is illustrated in figure 10.
In this case there exists a pseudo-saddle P_α close to the tangent point T_α. This is due to the changed location of P_α as compared to the case of BF_4. Increasing α for $\alpha < 0$, the points X_α, P_α and T_α approach each other and finally collide for $\alpha = 0$. After this collision there is only the invisible tangent point T_α left. For $\alpha > 0$, all solutions leave the neighborhood under consideration eventually.

Topological normal forms
The following topological normal forms serve as the simplest form of a Filippov system such that a certain bifurcation can be observed upon variation of the system parameter α. Every generic planar Filippov system satisfying the same bifurcation

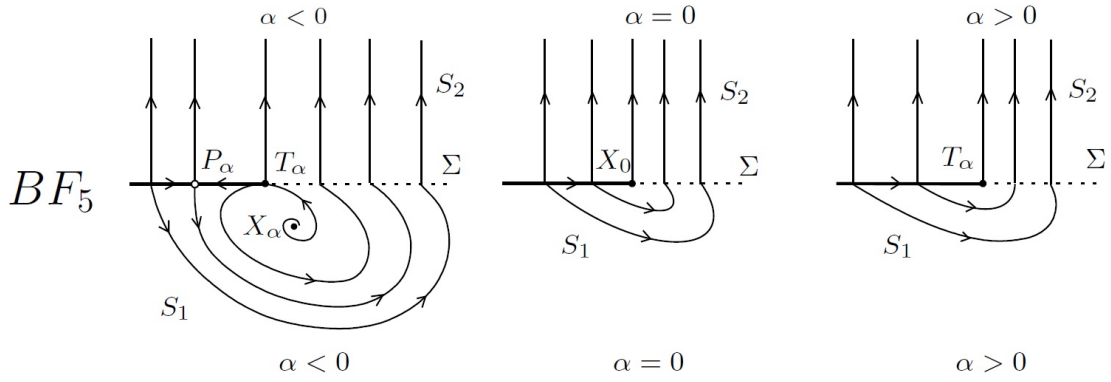

Figure 10: Boundary-focus-bifurcation of type BF_5. Source: Kuznetsov et al. (2003)[8]

classification criterion as its corresponding normal form is locally topologically equivalent to said normal form. Consider the system

$$\dot{\boldsymbol{x}} = \begin{cases} f^{(1)}(\boldsymbol{x}), & H(\boldsymbol{x}, \alpha) < 0 \\ f^{(2)}(\boldsymbol{x}), & H(\boldsymbol{x}, \alpha) > 0. \end{cases} \tag{8}$$

System (8) together with the vector fields listed in table 11 provide topological normal forms for each of the five cases, where $H(\boldsymbol{x}, \alpha) = x_2 + \alpha$. The local phase portraits in this section originate from these topological normal forms.

Type	$f^{(1)}(\boldsymbol{x})$	$f^{(2)}(\boldsymbol{x})$
BF_1	$\begin{pmatrix} x_1 - 2x_2 \\ 4x_1 \end{pmatrix}$	$\begin{pmatrix} 0 \\ -1 \end{pmatrix}$
BF_2	$\begin{pmatrix} x_1 - 2x_2 \\ 3x_1 \end{pmatrix}$	$\begin{pmatrix} 0 \\ -1 \end{pmatrix}$
BF_3	$\begin{pmatrix} -x_1 - 2x_2 \\ 4x_1 + 2x_2 \end{pmatrix}$	$\begin{pmatrix} 0 \\ -1 \end{pmatrix}$
BF_4	$\begin{pmatrix} x_1 - 2x_2 \\ 3x_1 \end{pmatrix}$	$\begin{pmatrix} 0 \\ 1 \end{pmatrix}$
BF_5	$\begin{pmatrix} -x_1 - 2x_2 \\ 4x_1 + 2x_2 \end{pmatrix}$	$\begin{pmatrix} 0 \\ 1 \end{pmatrix}$

Figure 11: Topological normal forms for the different types of the boundary focus bifurcation.

Boundary node bifurcation

The boundary node bifurcation refers to the collision of a stable or unstable node with the discontinuity boundary. In this discussion it is assumed that the colliding node X_α is stable. Two different types of boundary node bifurcations are to be considered. The two cases will be referred to as BN_1 and BN_2. The two types differ only by the direction of solutions in region S_2 as is illustrated in figure (12) and (13). All other imaginable scenarios involving the collision of a stable or unstable node can be reduced to the types BN_1 and BN_2.

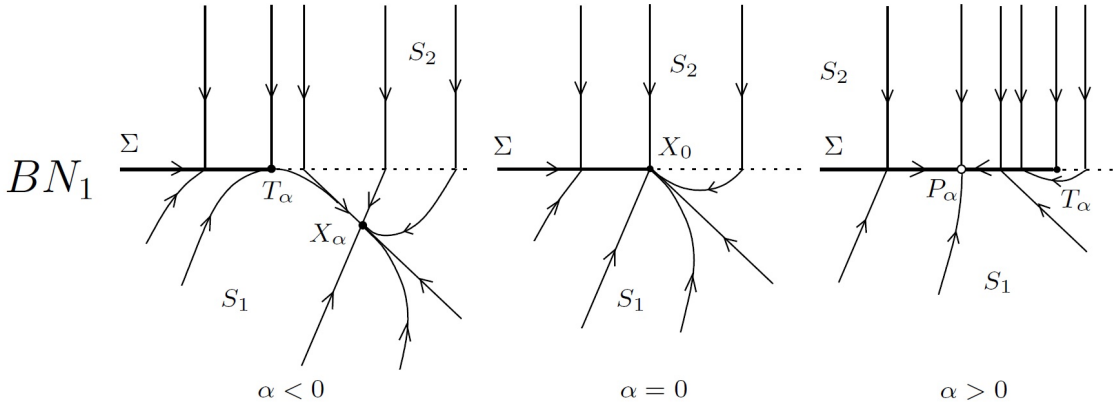

Figure 12: Boundary-node-bifurcation of type BN_1. Source: Kuznetsov et al. [8].

Similar as for the boundary focus bifurcation, there always exists a visible tangent point for $\alpha < 0$ and an invisible tangent point for $\alpha > 0$. For the type BN_1, the stable node X_α approaches the tangent point T_α, they collide for $\alpha = 0$ and form a boundary equilibrium X_0. Note that this boundary equilibrium is stable due to the orientation of solutions in S_2. For $\alpha > 0$ there exist now a stable pseudo-equilibrium and an invisible tangent point. This bifurcation shows how a stable node can turn into a stable pseudo-node upon collision with Σ. It shall be seen later that this particular situation can also be observed in the modified Rosenzweig-MacArthur model.

As was already indicated, the bifurcation types BN_1 and BN_2 differ only by the orientation of solutions in S_2. However, this seemingly minute difference has a profound impact on the outcomes of the bifurcation.

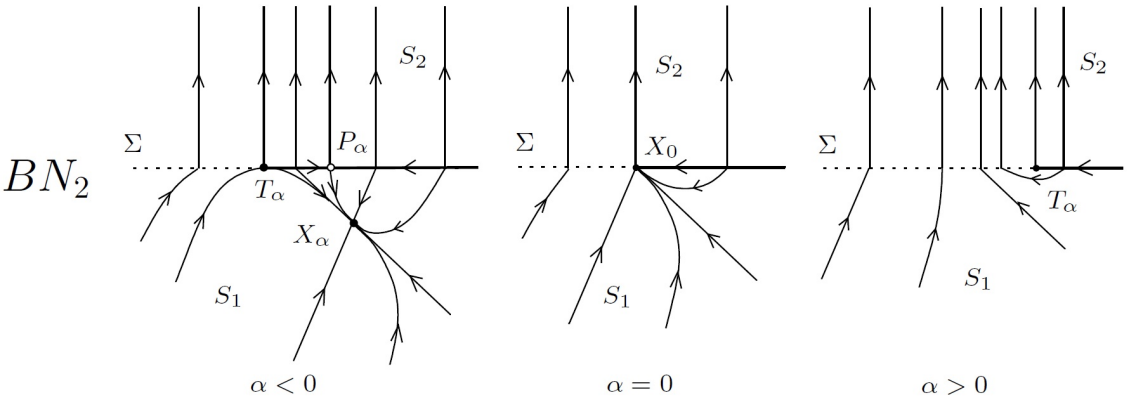

Figure 13: Boundary-node-bifurcation of type BN_2. Source: Kuznetsov et al. [8].

For the type BN_2, there exist a tangent point, the stable node and a pseudo-saddle P_α close to one another for $\alpha < 0$. When $\alpha = 0$, all three points collide into the boundary equilibrium X_0. It is interesting to note that even though X_0 is unstable there exists a whole range of orbits that tend to it. The basin of attraction is bounded by the non-leading stable line through X_0 and the sliding segment delimited by X_0. After the collision, for $\alpha > 0$, there only exists the now invisible tangent point T_α but no more attractors nearby.

Topological normal forms

Similarly as for the boundary focus normal forms, the system under consideration is system (8). The table below provides topological normal forms for the two cases, where it is assumed that $H(\boldsymbol{x}, \alpha) = x_2 + \alpha$. The local phase portraits shown in figure (12) and (13) are based on these normals forms.

Type	$f^{(1)}(\boldsymbol{x})$	$f^{(2)}(\boldsymbol{x})$
BN_1	$\begin{pmatrix} -3x_1 - x_2 \\ -x_1 - 3x_2 \end{pmatrix}$	$\begin{pmatrix} 0 \\ -1 \end{pmatrix}$
BN_2	$\begin{pmatrix} -3x_1 - x_2 \\ -x_1 - 3x_2 \end{pmatrix}$	$\begin{pmatrix} 0 \\ 1 \end{pmatrix}$

Figure 14: Topological normal forms for the two types of the boundary node bifurcation.

Pseudo-saddle-node bifurcation

Yet another kind of local bifurcation, which can be observed in the modified Rosenzweig-MacArthur system is the so called pseudo-saddle-node bifurcation. Two pseudo-equilibria can collide and annihilate each other upon variation of α. This bifurcation is completely analogue to the the standard saddle-node bifurcation. The phase portraits for a system displaying a pseudo-saddle-node bifurcation, as the parameter is varied from $\alpha < 0$, through $\alpha = 0$ and then to $\alpha > 0$ is illustrated in figure 15.

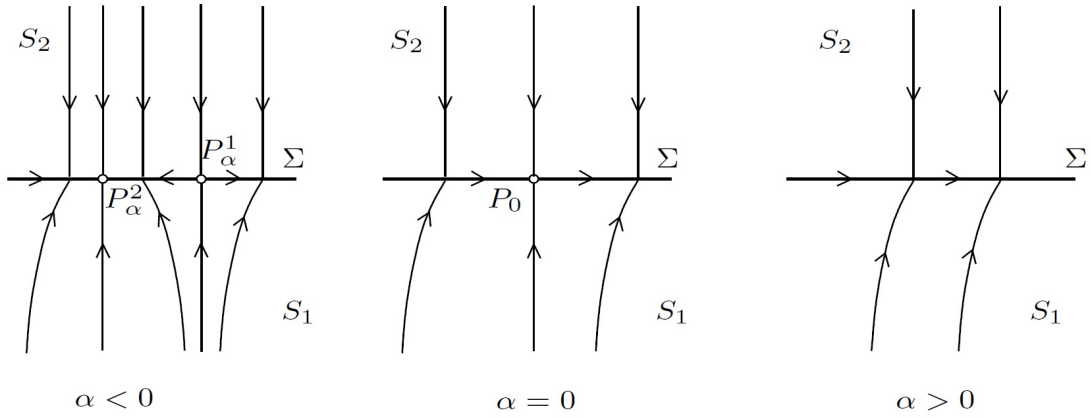

Figure 15: Pseudo-saddle-node bifurcation. Source: Kuznetsov et al. [8].

Figure 15 shows the collision of a stable pseudo-node with a pseudo-saddle. The pseudo-equilibria collide and disappear. For $\alpha = 0$, the point P_0 is called a *saddle-node*.

As already mentioned, there exist quite a few more types of local bifurcations that can occur in generic planar Filippov systems. Various types of collisions of tangent points are an example. These DIBs are not treated in this thesis as they cannot occur in the modified Rosenzweig-MacArthur model. However, the interested reader is encouraged to further study these DIBs. Starting points for further investigation

could be the article by Kuznetsov et al. [8] and the article by di Bernado, Budd, Champneys et al. [4].

4.2 Global Bifurcations

As will be soon evident, the modified Rosenzweig-MacArthur model displays two types of global bifurcations. The first one is due to the collision of the boundary with a limit cycle. Two other global bifurcations are characterized by the existence of sliding homoclinic orbits that that connect a pseudo-saddle to itself. In order to understand bifurcations involving periodic cycles it is important to understand what kinds of cycles can occur in such a system. In general there are three cases to be considered:

1. *Standard periodic solutions* are periodic solutions which are entirely contained in either region S_1 or S_2
2. *Sliding periodic solutions* are periodic solutions which partially slide on Σ_s.
3. *Crossing periodic solutions* are periodic solutions that cross Σ. Common points of Σ and solutions of this type are isolated points on Σ.

The orbits of these periodic solutions will be referred to as *standard cycle*, *sliding cycle* and *crossing cycle* respectively. It is very well possible for a crossing periodic solution to pass through a point which marks the boundary of a sliding segment. Due to the way that unique forward solutions were defined in chapter 3, it follows that sliding periodic solutions which share a common sliding segment must be the identical.

Stability of cycles:
The stability properties of periodic solutions are a critical aspect in the examination of DIBs involving cycles. Knowledge about the notion of a Poincaré map associated with a cycle is required. For a short introduction to Poincaré maps, the reader is referred to the appendix A.3.

(superstability) Consider a stable sliding cycle and introduce a local section to the orbit of the cycle. Now define a Poincaré map for forward time. The derivative of the Poincaré map is zero for the fixed point corresponding to the cycle. This is because all nearby points get mapped to the fixed point and the map is hence not invertible. To put this into a more geometric context; due to the overlapping of orbits on a sliding segment, every orbit to a solution that starts *sufficiently close* to the sliding cycle will eventually contain a point that lies *on* the sliding cycle. This happens in finite time. Kuznetsov et al. refer to this phenomenon as *superstability* in section 4 of their article [8]. It can be shown that a crossing cycle passing through the boundary of a sliding segment is always superstable from the inside and from the outside.

(exponential stability) For a generic crossing cycle the Poincaré map is smooth and invertible. If $P'(\boldsymbol{x})$ is the derivative of the Poincaré map evaluated at the fixed point corresponding to the cycle, then the crossing cycle is exponentially stable if $P'(\boldsymbol{x}) < 1$ and exponentially unstable for $P'(\boldsymbol{x}) > 1$ (see appendix A).

More complicated behaviours of sliding and crossing cycles, involving multiple sliding segments and crossings are possible. However, for the purposes of this thesis it will suffice to consider only the simplest cases.

Touching bifurcation

The collision of a piece of a cycle with the discontinuity boundary is most commonly referred to as *touching* or *grazing bifurcation*. The following situation will be of consideration: A cycle touches the sliding segment Σ_s at a quadratic tangent point T_0 for $\alpha = 0$. The cycle which exists just when the cycle touches Σ_s, i.e. for $\alpha = 0$, is called the *touching cycle*. Depending on the stability properties of this touching cycle, there are two different types of touching bifurcations. For the type TC_1, the touching cycle is stable whereas for type TC_2, the touching cycle is unstable. This leads to two very different outcomes of the bifurcations.

Type TC_1: The phase portraits for a system displaying a touching bifurcation of type TC_1, as the parameter is varied from $\alpha < 0$, through $\alpha = 0$ and then to $\alpha > 0$ is illustrated in figure 16.

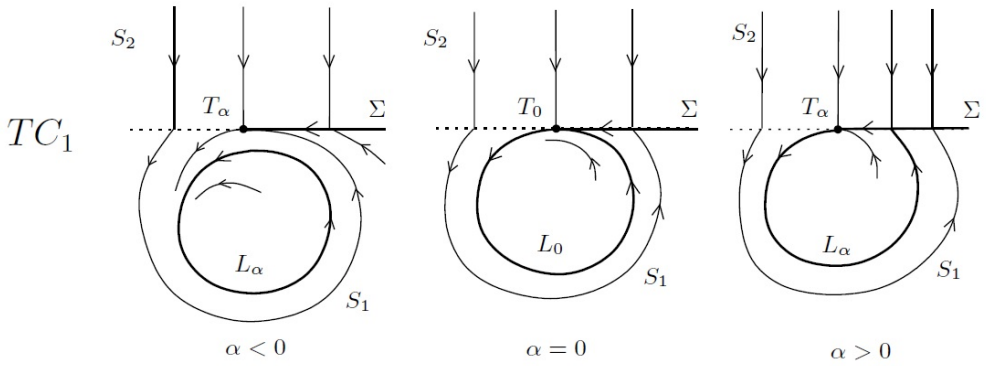

Figure 16: Touching bifurcation of type TC_1. The cycle L_α changes stability from exponential stability to superstability. Source: Kuznetsov et al. [8]

As can be seen in figure 16, the exponentially stable standard cycle L_α is a distance $O(\alpha)$ from Σ for $\alpha < 0$. The cycle collides with Σ for $\alpha = 0$ with non-zero velocity with respect to α. For $\alpha > 0$ the standard cycle has turned into a sliding cycle and changed its stability from exponentially stable to superstable.

Type TC_2: The phase portraits for a system displaying a touching bifurcation of type TC_2, as the parameter is varied from $\alpha < 0$, through $\alpha = 0$ and then to $\alpha > 0$ is shown in figure 17. In the case of a bifurcation of type TC_2, it is first to be observed that there exist two cycles for $\alpha < 0$. The presence of the unstable standard cycle L^u_α has the effect that the special orbit exiting from T_α re-enters into the sliding segment and forms a superstable sliding cycle L^s_α. As α approaches zero, L^u_α approaches Σ and L^s_α shrinks around L^u_α until they coincide in the touching cycle L_0 for $\alpha = 0$. For $\alpha > 0$ no more cycles exist. This is strongly resembles the standard saddle-node-bifurcation but now for periodic cycles.

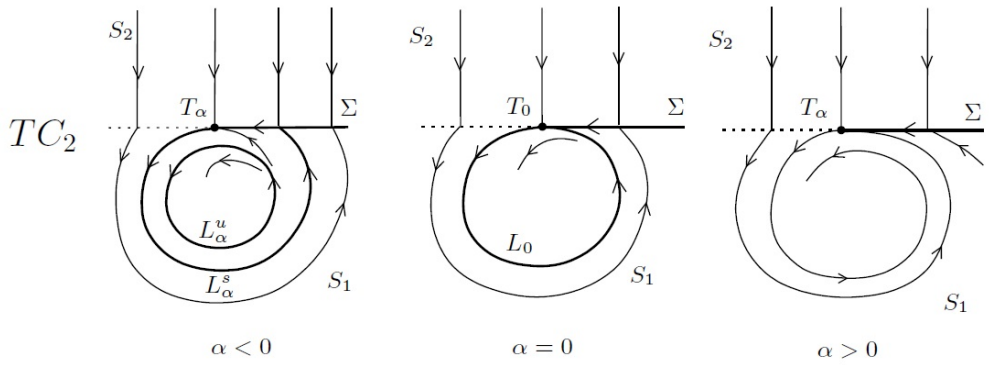

Figure 17: Touching bifurcation of type TC_2. Two cycles coincide in a touching cycle and annihilate each other. Source: Kuznetsov et al. [8].

Pseudo-homoclinic bifurcation

A pseudo-homoclinic bifurcation is characterized by the appearance of a homoclinic orbit that somehow interacts with the discontinuity boundary Σ. This can happen in three ways. The first one is the connection of a pseudo-saddle-node to itself. The second is the connection of a pseudo-saddle to itself. Finally, the third is the homoclinic connection of a standard saddle to itself which happens to contain a sliding segment. The only one of relevance to this thesis is the second one, the homoclinic connection from a pseudo-saddle to itself.

Homoclinic connection for a pseudo-saddle

The phase portraits for a system displaying the appearance of a homoclinic connection from a pseudo-saddle to itself, as the parameter is varied from $\alpha < 0$, through $\alpha = 0$ and then to $\alpha > 0$ are illustrated in figure 18:

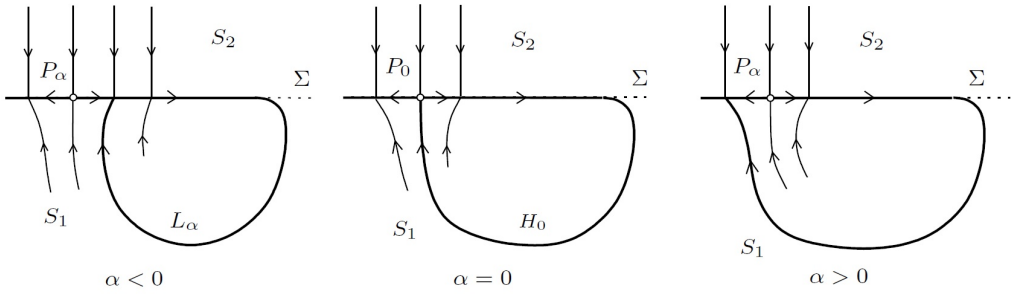

Figure 18: Homoclinic connection from a pseudo-saddle to itself. Source: Kuznetsov et al. [8].

In this bifurcation, a sliding cycle L_α collides with a pseudo-saddle P_α. As can be seen in figure 18, for $\alpha \to 0^-$, the sliding cycle approaches the pseudo saddle P_α. For $\alpha = 0$, the collision occurs and the homoclinic connection H_0 exists. For small $\alpha > 0$ the homoclinic connection disappears. This bifurcation is completely analogue to the standard homoclinic bifurcation when a standard cycle collides with a standard saddle.

Pseudo-heteroclinic bifurcation

A pseudo-heteroclinic connection is an orbit that connects a pseudo-equilibrium to a different pseudo-equilibrium or a regular equilibrium. These connections are completely analogue to their counterparts for smooth systems and are only mentioned for the sake of completeness. There are two different heteroclinic connections that can be observed in the modified Rosenzweig-MacArthur model. The first one is the connection of a standard saddle to a pseudo-node and the second one is the connection of a standard saddle to a pseudo-saddle-node.

Various other global bifurcations are excluded from this thesis as they cannot be observed in the modified Rosenzweig-MacArthur model. Examples of such bifurcations are what Kuznetsov et. al. refer to as *buckling* and *crossing*. These belong to the class of bifurcations of cycles and describe what happens if a special orbits returns to an invisible tangent point or when a special orbit leaves and returns to the sliding segment through the same visible tangent point. The interested reader is again referred to articles [8] and [4]. Having discussed the theory for all relevant bifurcations it is now time to apply the knowledge gained in the past two chapters. In the following chapter we will see how all the concepts discussed this far come together and can be used to investigate population-density-dependent harvesting in a modified Rosenzweig-MacArthur model.

5 Application to a Predator-Prey Model

In this section, we will see how all the discussed theory about Filippov Systems and the bifurcations occurring in these systems can be applied to a modified version of the Rosenzweig-MacArthur model.

5.1 Modifying the Rosenzweig-MacArthur Model

Recall that after the rescaling process, the system equations were found to be:

$$\dot{x}_1 = x_1(1 - x_1) - \frac{ax_1x_2}{b + x_1},$$
$$\dot{x}_2 = \frac{ax_1x_2}{b + x_1} - dx_2,$$

where a, b and d are positive parameters. Now the harvesting of predators is introduced for $x_2 > \alpha$. In terms of the equations, this means that for $x_2 > \alpha$ the mortality rate changes from $-d$ to $-(d + E)$, where $E > 0$ represents the harvesting effort. The resulting vector field is discontinuous along the line $x_2 = \alpha$ and hence, the system is a Filippov system. In the following discussion, the parameters a, b, d and E will be assigned certain values. The only system parameter left will be α. The dynamics of this family of Filippov systems is given by

$$\dot{\boldsymbol{x}} = \begin{cases} f^{(1)}(\boldsymbol{x}), & \boldsymbol{x} \in S_1, \\ f^{(2)}(\boldsymbol{x}), & \boldsymbol{x} \in S_2. \end{cases} \tag{9}$$

The partitioning of the first quadrant into the regions S_1, S_2 and Σ is illustrated in figure 19.

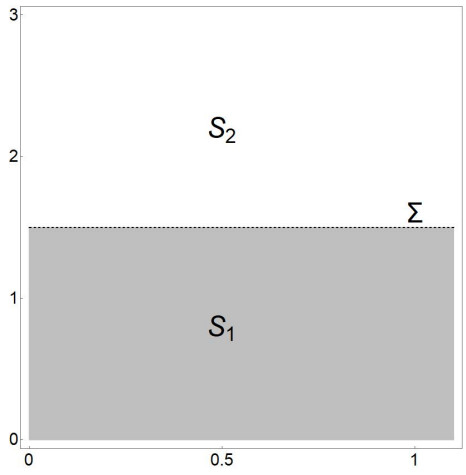

Figure 19: Partitioning of the phase space for $\alpha = 1.5$.

The regions S_1 and S_2 are again expressed using the function $H(\boldsymbol{x}, \alpha)$.

$$S_1 = \{\boldsymbol{x} \in \mathbb{R}^2 : H(\boldsymbol{x}) < 0 \text{ and } x_1, x_2 \geq 0\},$$
$$S_2 = \{\boldsymbol{x} \in \mathbb{R}^2 : H(\boldsymbol{x}) > 0 \text{ and } x_1, x_2 \geq 0\},$$
$$\Sigma = \{\boldsymbol{x} \in \mathbb{R}^2 : H(\boldsymbol{x}) = 0 \text{ and } x_1, x_2 \geq 0\}.$$

In the system at hand, the discontinuity in the vector field occurs along the line $x_2 = \alpha$ and hence

$$H(\boldsymbol{x}, \alpha) = x_2 - \alpha,\ \alpha > 0,$$

is a suitable choice for the function H. It is assumed that $\alpha > 0$. This is because the case $\alpha = 0$ would correspond to just another continuous system with a different natural death rate. The dynamics on S_1 and S_2 is given by

$$f^{(1)}(\boldsymbol{x}) = \begin{bmatrix} x_1(1-x_1) - \frac{ax_1x_2}{b+x_1} \\ \frac{ax_1x_2}{b+x_1} - dx_2 \end{bmatrix}, \qquad f^{(2)}(\boldsymbol{x}) = \begin{bmatrix} x_1(1-x_1) - \frac{ax_1x_2}{b+x_1} \\ \frac{ax_1x_2}{b+x_1} - (d+E)x_2 \end{bmatrix}.$$

Recall that in section 3.2 the sliding set Σ_s was defined as the set of all points on Σ such that $\sigma(\boldsymbol{x}) \leq 0$. For this system, $\sigma(\boldsymbol{x})$ is given by

$$\begin{aligned} \sigma(\boldsymbol{x}) &= \langle \nabla H(\boldsymbol{x}), f^{(1)}(\boldsymbol{x}) \rangle \langle \nabla H(\boldsymbol{x}), f^{(2)}(\boldsymbol{x}) \rangle \\ &= \left(\frac{a\alpha x_1}{b+x_1} - d\alpha \right) \left(\frac{a\alpha x_1}{b+x_1} - (d+E)\alpha \right). \end{aligned}$$

Imposing $\sigma(\boldsymbol{x}) \leq 0$ and solving for x_1 yields that

$$\Sigma_s = \{ \boldsymbol{x} \in \Sigma | \frac{bd}{a-d} \leq x_1 \leq \frac{b(d+E)}{a-(d+E)} \}.$$

This implies that Σ_s consists of a unique sliding segment which is the line segment between and including the points $(\frac{bd}{a-d}, \alpha)$ and $(\frac{b(d+E)}{a-(d+E)}, \alpha)$. From now on, whenever Σ_s is mentioned, the reader should interpret this as "the unique sliding segment in Σ_s".

The next step is now to find the equation describing the dynamics on Σ_s. To do this, Filippov's convex method as discussed in section 3.2 will be employed. Recall that we are interesting in finding $g(\boldsymbol{x})$ which is the unique linear convex combination of $f^{(1)}(\boldsymbol{x})$ and $f^{(2)}(\boldsymbol{x})$, tangent to Σ. Note that since $H(\boldsymbol{x}, \alpha) = x_2 - \alpha$, it follows that

$$\nabla_{\boldsymbol{x}} H = \begin{bmatrix} 0 \\ 1 \end{bmatrix},$$

and hence

$$\lambda = \frac{\langle \nabla_{\boldsymbol{x}} H(\boldsymbol{x}), f^{(2)}(\boldsymbol{x}) \rangle}{\langle \nabla_{\boldsymbol{x}} H(\boldsymbol{x}), f^{(2)}(\boldsymbol{x}) - f^{(1)}(\boldsymbol{x}) \rangle} = \frac{-ax_1}{E(b+x_1)} + \frac{d+E}{E}.$$

Using λ, the function $g(\boldsymbol{x})$, which describes the dynamics on the sliding segment of Σ_s, is given by

$$g(\boldsymbol{x}) = \lambda f^{(1)}(\boldsymbol{x}) + (1-\lambda) f^{(2)}(\boldsymbol{x}) = \begin{bmatrix} x_1 \left(1 - x_1 - \frac{a\alpha}{b+x_1} \right) \\ 0 \end{bmatrix} \tag{10}$$

Observe that the x_1-component of $g(\boldsymbol{x})$ is exactly the x_1-component of the vector fields $f^{(1)}(\boldsymbol{x})$ and $f^{(2)}(\boldsymbol{x})$. This makes a lot of sense considering that $f^{(1)}$ and $f^{(2)}$ have the same x_1-components and that $g(\boldsymbol{x})$ is the unique linear convex combination of $f^{(1)}$ and $f^{(2)}$ tangent to Σ. Here "tangent to Σ" means "has zero x_2-component", since Σ is given by a line of constant x_2. It follows that finding $g(\boldsymbol{x})$ effectively boils

down to a projection of $f^{(1)}$ (or $f^{(2)}$) onto the x_1-axis, which is reflected in equation (10). Moreover, note that

$$g(\boldsymbol{x}) = g^*(x_1)$$

does only depend on x_1. This means that we can treat the dynamics on Σ_s as a one-dimensional system.

We will soon see that knowledge about the nullclines will prove to be very helpful in the detection of DIBs. The x_1-nullclines of system (9) are

$$N_1 = \{\boldsymbol{x} \in \mathbb{R}^2 |\ x_1 = 0\},$$
$$N_2 = \{\boldsymbol{x} \in \mathbb{R}^2 |\ x_2 = \frac{1}{a}(1 - x_1)(b + x_1)\},$$

and the x_2-nullclines are given by

$$N_3 = \{\boldsymbol{x} \in \mathbb{R}^2 |\ x_2 = 0\},$$
$$N_4 = \{\boldsymbol{x} \in \mathbb{R}^2 |\ x_1 = \frac{bd}{a-d}, x_2 \leq \alpha\},$$
$$N_5 = \{\boldsymbol{x} \in \mathbb{R}^2 |\ x_1 = \frac{b(d+E)}{a-(d+E)}, x_2 \geq \alpha\}.$$

Note that due to the division of the first quadrant into S_1 and S_2, the nontrivial x_2-nullcline now is also divided up into two pieces (N_4 and N_5). Since the discontinuity boundary Σ is given by a half-line of constant $x_2 = \alpha$, it follows that tangent points on Σ can only occur when the x_2-component of $f^{(1)}$ or $f^{(2)}$ is zero. Hence tangent points occur at the intersections of the x_2-nullclines with Σ and it follows that there are only two tangent points, namely

$$T_1 = (\frac{bd}{a-d}, \alpha) \qquad \text{and} \qquad T_2 = (\frac{b(d+E)}{a-(d+E)}, \alpha).$$

These correspond to the intersections of N_4 and N_5 with Σ_s and already showed up in the discussion of the uniqueness of the sliding segment Σ_s. To give a bit of a feeling for what phase portraits and nullclines for this family of Fillipov systems look like, two phase portraits are given in figure 20.

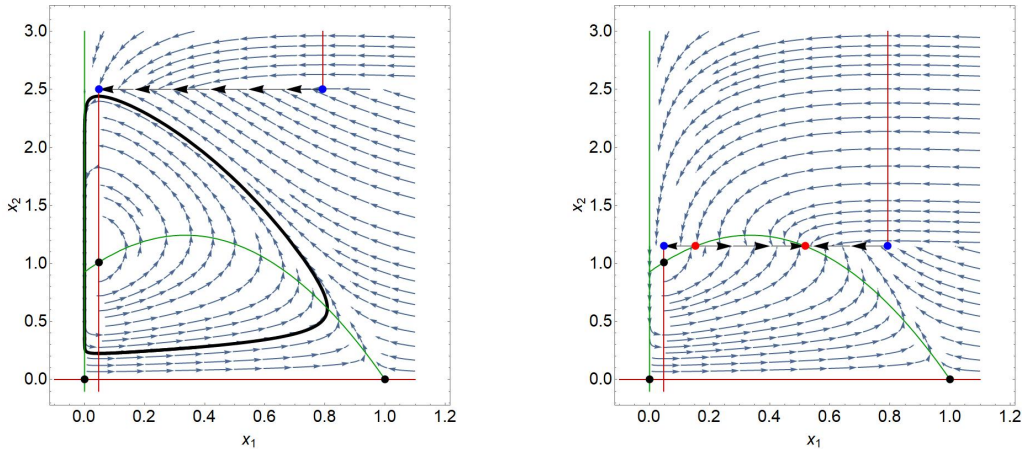

Figure 20: Phase portrait for the Filippov system for $\alpha = 2.5$ (left) and $\alpha = 1.15$ (right). The remaining system parameters are set to $a = 0.3556$, $b = 0.33$, $d = 0.0444$ and $E = 0.2067$.

The sliding segment is depicted as a black line and the flow on the sliding segment is indicated by black arrows. Standard equilibria are indicated with a black dot, pseudo-equilibria are shown as red dots and tangent points are represented by blue dots. The x_1-nullclines are the lines in green and the x_2-nullclines are the lines in red. As can be seen, for relative large α values there exists a periodic orbit in region S_1. This periodic orbit disappears when α decreases as can be seen from figure 20. How exactly this happens and what other bifurcations occur will be investigated now.

All types of local bifurcations, i.e. collisions of pseudo-equilibria, boundary-equilibria and tangent points can be examined by investigating the system

$$\dot{x}_1 = g^*(x_1),\ x_1 \in \left[\frac{bd}{a-d}, \frac{b(d+E)}{a-(d+E)}.\right]$$

This can be considered a one-dimensional system and hence the bifurcation analysis with respect to α will be rather straightforward. At the same time, the full characterization of bifurcation behaviour of this system with respect to a, b, d, E and α is very intricate. As was indicated in section 2, there occurs a Hopf bifurcation for $b = \frac{a-d}{a+d}$ in the continuous Rosenzweig-MacArthur model. The discussion of the various interactions of such a Hopf bifurcation with the discontinuity boundary is not included in this thesis. Instead, the parameters a, b, d and E will be fixed. The only system parameter left will be α and the bifurcation analysis will be done with respect to α. Two different parameter configurations of a, b, d and E are to be considered, of which the first configuration is $a = 0.3556$, $b = 0.33$, $d = 0.0444$ and $E = 0.2067$. This corresponds to the case $b < \frac{a-d}{a+d}$ and hence for large α, a periodic solution will be present in the region S_1. This parameter configuration has been taken from article [8] and it will be attempted to replicate their findings. The second parameter configuration is $a = 0.3, b = 0.4, d = 0.15$ and $E = 0.05$, which corresponds to the case where $b > \frac{a-d}{a+d}$ and hence no periodic solution will exist in S_1. This parameter setting was chosen to be somewhat comparable to the first parameter configuration while representing the case $b > \frac{a-d}{a+d}$. Additionally, the chosen values are relatively simple to work with and simplify the making of clear phase portraits so that the two cases can be compared more easily. Local and global bifurcations will be discussed for the two parameter settings.

5.2 Bifurcations for the Case: $\mathbf{b < \frac{a-d}{a+d}}$

To represent the case $b < \frac{a-d}{a+d}$, the parameters are set to $a = 0.3556$, $b = 0.33$, $d = 0.0444$ and $E = 0.2067$.

Local Bifurcations

Recall that the dynamics on Σ_s is given by $\dot{\boldsymbol{x}} = g(\boldsymbol{x})$. Now to find equilibria of this system we set

$$g(\boldsymbol{x}) = \begin{bmatrix} x_1\left(1 - x_1 - \frac{a\alpha}{b+x_1}\right) \\ 0 \end{bmatrix} = \mathbf{0}.$$

If x_1^* is a solution to $x_1\left(1 - x_1 - \frac{a\alpha}{b+x_1}\right) = 0$, then (x_1^*, α) is a pseudo- or boundary-equilibrium of the system at hand. Figure 21 shows the dependence of pseudo-equilibria on α.

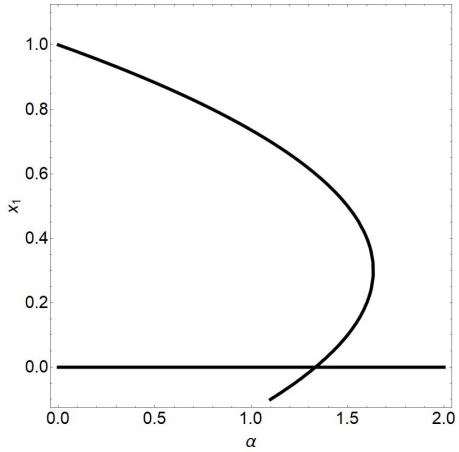

Figure 21: Bifurcation diagram for the dynamics on Σ_s showing α on the horizontal axis and x_1 on the vertical axis.

Pseudo-Saddle-Node. Examining the equation

$$x_1 \left(1 - x_1 - \frac{a\alpha}{b + x_1}\right) = 0$$

and the bifurcation diagram in figure 21, there are two values of α which seem particularly interesting. The first one is the intersection of the line $x_1 = 0$ with the parabola

$$\left(1 - x_1 - \frac{a\alpha}{b + x_1}\right) = 0. \tag{11}$$

The second point of interest is the vertex of the aforementioned parabola. The function $g(\boldsymbol{x})$ describes how solutions behave on sliding segments of Σ_s which is delimited by the tangent points T_1 and T_2. Since both tangent points always have positive x_1-components, it follows that $g(\boldsymbol{x})$ cannot possibly dictate the behaviour of a solution at $x_1 = 0$. This means that investigating the intersection of the parabola and the line $x_1 = 0$ does not yield any meaningful insights.

Very differently so for the vertex of the parabola (11). The vertex is given by

$$(x_1, x_2) = (\frac{1-b}{2}, \frac{(b+1)^2}{4a}). \tag{12}$$

This corresponds exactly to the moment at which the discontinuity boundary touches the maximum of the nontrivial x_1-nullcline

$$x_2 = \frac{1}{a}(1 - x_1)(b + x_1).$$

Again by inspection of figure 21 and under consideration of the equation (11), one might suspect that there occurs a saddle-node-bifurcation at the point indicated in (12). To verify this, it is convenient to make use of the following theorem.

Theorem. *If $\dot{x} = f(x, \alpha)$ is a first-order differential equation such that*

1. $f(\hat{x}, \alpha_0) = 0$,
2. $\frac{\partial f}{\partial x}(\hat{x}, \alpha_0) = 0$,

3. $\frac{\partial^2 f}{\partial x^2}(\hat{x}, \alpha_0) \neq 0$,

4. $\frac{\partial f}{\partial \alpha}(\hat{x}, \alpha_0) \neq 0$,

then this differential equation undergoes a saddle-node bifurcation at $\alpha = \alpha_0$.

A very intuitive proof of this result can be found in chapter 8 of the book *Differential Equations, Dynamical Systems and an Introduction to Chaos* by Devaney, Hirsch and Smale [6].

The next step is to find the corresponding derivatives for the system at hand and then substitute $\hat{x}_1 = \frac{1-b}{2}$ and $\alpha_0 = \frac{(b+1)^2}{4a}$ to see if the conditions for the above theorem are met. Computing the derivatives and substitution yields

1. $f(\hat{x}, \alpha_0) = 0 = x\left(1 - x - \frac{a\alpha}{b+x}\right)\Big|_{\hat{x},\alpha_0} = 0$,

2. $\frac{\partial f}{\partial x}(\hat{x}, \alpha_0) = 1 - 2x - \frac{a\alpha b}{(b+x)^2}\Big|_{\hat{x},\alpha_0} = 0$,

3. $\frac{\partial^2 f}{\partial x^2}(\hat{x}, \alpha_0) = -2 + \alpha\frac{2ab}{(b+x)^3}\Big|_{\hat{x},\alpha_0} = 2\frac{b-1}{b+1}$,

4. $\frac{\partial f}{\partial \alpha}(\hat{x}, \alpha_0) = -\frac{ax}{b+x}\Big|_{\hat{x},\alpha_0} = \frac{a(b-1)}{b+1}$.

Note that it seems that the first two conditions are always met whereas the third and fourth condition are met *if and only if* $b \neq 1$. In the case that $b = 1$, the discontinuity boundary would touch the maximum of the nontrivial x_1-nullcline at the point $(x_1, x_2) = (0, \frac{1}{a})$. This point does not lie on the line segment between the tangent points T_1 and T_2 and is hence not contained in the sliding segment in Σ_s.

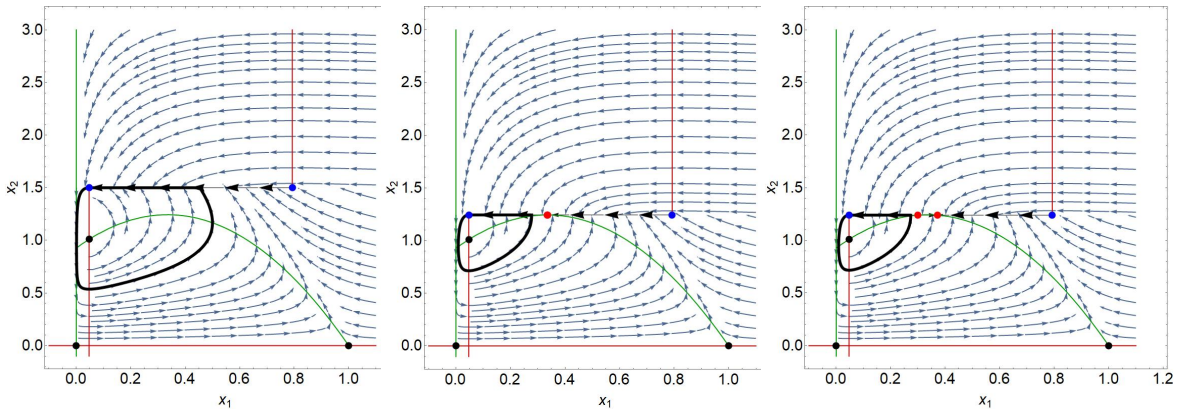

Figure 22: Phase portraits before, at and after the pseudo-saddle-node bifurcation. The parameter values are $\alpha = 1.5$, $\alpha_0 \approx 1.2436$ and $\alpha = 1.24$ (left to right).

It follows that conditions 3 and 4 are also always met since it would not make any sense to speak of bifurcations of the system

$$\dot{x}_1 = x_1\left(1 - x_1 - \frac{a\alpha}{b + x_1}\right)$$

which *do not lie* on Σ_s. So indeed, there occurs a saddle-node bifurcation on the sliding segment for

$$\alpha_{PSN} = \frac{(b+1)^2}{4a} = 1.2436.$$

The phase portraits before, during and after this bifurcation are given in figure 22. As discussed in chapter 4, since this saddle-node-bifurcation is due to the sliding dynamics and occurs on Σ_s, this bifurcation is called a *pseudo-saddle-node* bifurcation.

Boundary Focus. Having discussed local bifurcations that occur due to the dynamics on Σ_s itself, it is now time to investigate local bifurcations that occur due to the collision of standard equilibria with Σ_s. As was shown in section 2, there are three standard equilibria to be considered, namely the points $(0,0)$, $(1,0)$ and the coexistence equilibrium

$$\Big(\frac{bd}{a-d}, \frac{b(a-bd-d)}{(a-d)^2}\Big).$$

The equilibria $(0,0)$ and $(1,0)$ do not collide with Σ as it was assumed that $\alpha > 0$. There are two collisions that need to be investigated. The first one is a boundary focus bifurcation and corresponds to the α value such that the tangent point T_1 lies on the nontrivial x_1-nullcline. The other collision is a boundary node bifurcation, which is marked by T_2 lying on the nontrivial x_1-nullcline.

Let us first consider the collision of the coexistence equilibrium with the sliding segment Σ_s. The coexistence equilibrium is an unstable focus. In order to classify its collision with Σ_s as one of the five forms of the boundary-focus bifurcation known from chapter 4, it is necessary to check a number of things.

Assume that the collision of the unstable focus occurs for some $\alpha = \alpha_0$. The inspection of figure 23 indicates that the orientation of solutions in S_2 close to the coexistence equilibrium is downward when $\alpha \approx \alpha_0$. Further, it is evident from the discussion of the pseudo-saddle-node bifurcation that for $\alpha \approx \alpha_0$ there is a pseudo-saddle nearby which collides with the coexistence equilibrium and T_1 for $\alpha = \alpha_0$. These observations already exclude the types BF_3, BF_4 and BF_5.

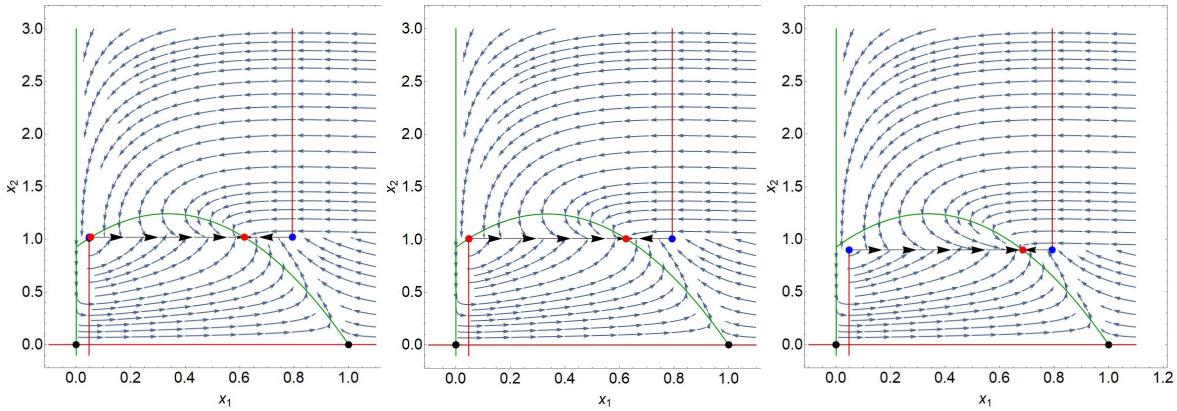

Figure 23: Phase portraits before, at and after the boundary focus bifurcation. The parameter values are $\alpha = 1.02$, $\alpha_0 \approx 1.0105$ and $\alpha = 0.9$ (left to right). Note that there is a very small sliding cycle present in the phase portrait on the left.

In order to determine whether the bifurcation is of type BF_1 or BF_2, the method for the analytic distinction of these two types, as described in chapter 4, will be

employed: The system

$$\dot{\boldsymbol{x}} = f^{(1)}(\boldsymbol{x})$$

is linearized around the focus equilibrium. The resulting linearized system is given by

$$\dot{\boldsymbol{x}} = \begin{bmatrix} a^* & b^* \\ c^* & d^* \end{bmatrix} \boldsymbol{x} = \begin{bmatrix} -\frac{d(ab-a+bd+d)}{a(a-d)} & -d \\ \frac{a-bd-d}{a} & 0 \end{bmatrix} \boldsymbol{x}.$$

Now a solution to this linearized system, starting at $(-\frac{d^*}{c^*}, 1)$, is determined numerically. The point at which this solution intersects the line $x_2 = 1$ again for the first time is $(\theta, 1)$ and we compare where this point lies relative to $(-\frac{b}{a}, 1)$. The numerical analysis shows that $\theta < -\frac{b}{a}$ and hence the bifurcation is of type BF_1. A more detailed description of the numerical results can be found in appendix B. The α value of the collision can be found by evaluating the nontrivial x_1-nullcline at the x_1-coordinate of T_1:

$$\alpha_{BF} = \frac{b(a-bd-d)}{(a-d)^2} = \frac{771}{763} \approx 1.0105.$$

Boundary Node. The last local bifurcation that occurs for this parameter configuration is the boundary node bifurcation which corresponds to the collision of T_2 with the nontrivial x_1-nullcline. As α decreases after the pseudo-saddle-node bifurcation, the newly generated pseudo-node wanders along the nontrivial x_1-nullcline until it collides with T_2 into a boundary equilibrium. The α value of the collision can be found by evaluating the nontrivial x_1-nullcline at the x_1-coordinate of T_2.

$$\alpha_{BN} = \frac{b\left[a - b(d+E) - (d+E)\right]}{(a-(d+E))^2} = \frac{5901}{9025} \approx 0.6539$$

As was shown in chapter 2, the coexistence equilibrium in the continuous Rosenzweig-MacArthur model is a sink for $b > \frac{a-d}{a+d}$. In the discussion of the trace and determinant of the linearization around this equilibrium it was also shown that this sink can be a focus or a node, depending on the specific parameter configuration. For the parameter values as set in the beginning of this subsection, the coexistence equilibrium in S_2 is indeed a stable node. This can easily be verified by computing the eigenvalues of the corresponding linearization matrix. The equilibrium is given by

$$(\bar{x}_1, \bar{x}_2) = \Big(\frac{b(d+E)}{a-(d+E)}, \frac{b(a-b(d+E)-(d+E))}{(a-(d+E))^2}\Big),$$

and hence

$$J(\bar{x}_1, \bar{x}_2) = \begin{bmatrix} 1 - 2\bar{x}_1 - \frac{ab\bar{x}_2}{(b+\bar{x}_1)^2} & -\frac{a\bar{x}_1}{b+\bar{x}_1} \\ \frac{ab\bar{x}_2}{(b+\bar{x}_1)^2} & 0 \end{bmatrix} = \begin{bmatrix} -\frac{1677}{2593} & -\frac{856}{3409} \\ -\frac{1557}{25589} & 0 \end{bmatrix}.$$

The eigenvalues are

$$\lambda_1 = -\frac{746}{1199} \text{ and } \lambda_2 = -\frac{101}{4113}.$$

Both eigenvalues are real and negative, hence the equilibrium is a stable node and the collision is indeed a boundary node bifurcation and not a boundary focus bifurcation.

Now that we know that we are dealing with a a boundary node bifurcation, the next step is to classify this bifurcation to be of type BN_1 or BN_2. Since this boundary

node bifurcation involves the collision of a stable pseudo-node with a tangent point, the bifurcation can only possibly be of type BN_1. The local phase portrait can be obtained from the BN_1 normal form, discussed in section 4 by considering a reversed order of the images and renaming the regions S_1 and S_2. The phase portraits before, during and after the boundary-node bifurcation are given in figure 24.

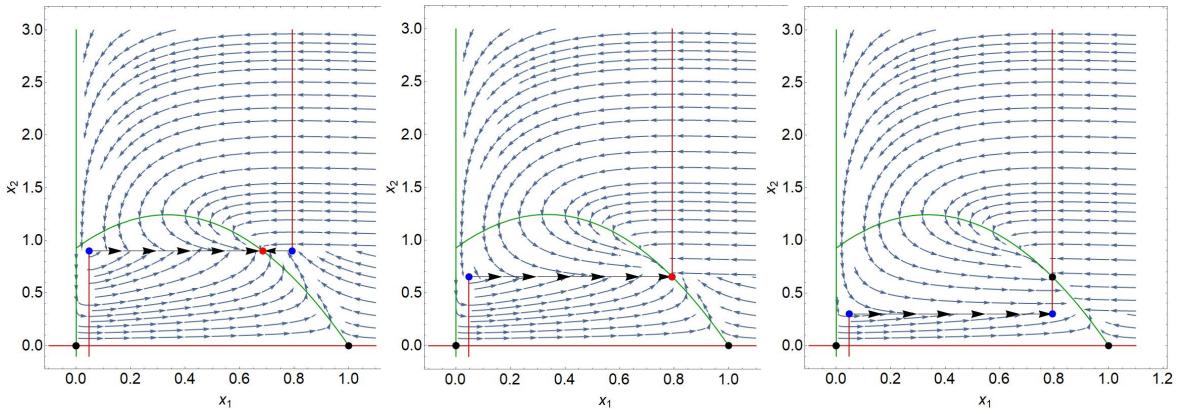

Figure 24: Phase portraits before, at and after the boundary-node bifurcation. The parameter values are $\alpha = 0.9$, $\alpha_0 \approx 0.6539$ and $\alpha = 0.3$ (left to right).

Global Bifurcations

The detection of global bifurcations will largely be done numerically. Recall that for $b < \frac{a-d}{a+d}$ there exists a periodic solution in the region S_1. By inspecting the phase portraits, it is clear that for large α, that is for $\alpha > 2.5$, there cannot exist any global bifurcations as there are no interactions of Σ_s and the periodic orbit, nor can there be interactions with the pseudo-equilibria. The first global bifurcation that occurs is hence the collision of the standard periodic orbit in S_1 with Σ_s.

Touching bifurcation. When decreasing α, the periodic orbit collides with the tangent point T_1 and becomes a sliding cycle. Looking at the phase portraits only, one might assume that this sliding cycle exists until the boundary focus bifurcation occurs but we will soon see that this is not the case. This touching bifurcation is of type TC_1 as the colliding periodic orbit is stable. To find an approximation of the α value for which this touching bifurcation occurs, a solution to the system

$$\dot{\boldsymbol{x}} = f^{(1)}(\boldsymbol{x}), \;\; \boldsymbol{x} \in \{(x_1, x_2) \in \mathbb{R}^2 | x_1, x_2 > 0\}$$

is computed numerically. For the corresponding Matlab code and a short explanation of the method employed, the reader is referred to appendix B. The approximate value at which the touching bifurcation occurs is $\alpha_{TC} \approx 2.4405$. The phase portraits before, during and after this bifurcation are given in figure 25. What happens when α decreases even further will be discussed in the following paragraphs on pseudo-homoclinic connections.

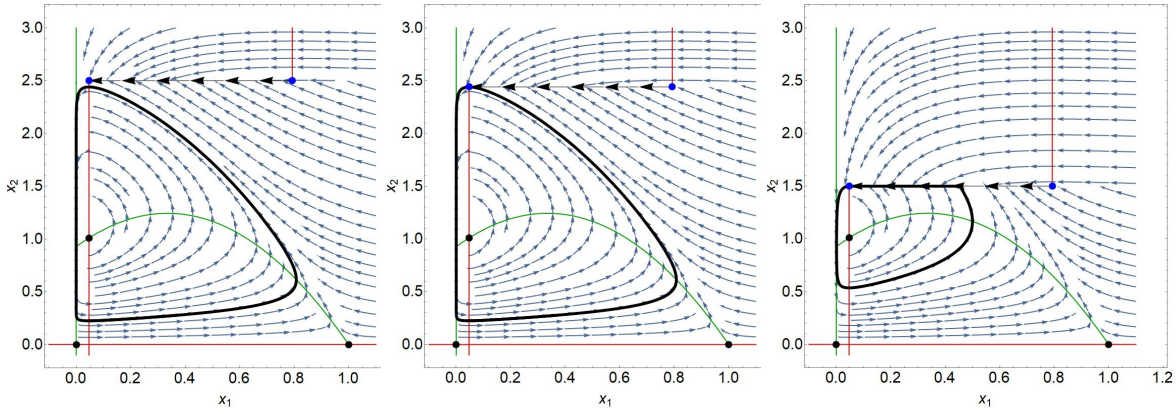

Figure 25: Phase portraits before, at and after the touching bifurcation. The parameter values are $\alpha = 2.5$, $\alpha_0 \approx 2.4405$ and $\alpha = 1.5$ (left to right).

Pseudo-homoclinic bifurcations. As was discussed in chapter 4 there are three ways that pseudo-homoclinic connections can come into existence. The first one is the connection of a pseudo-saddle-node to itself, the second one is the connection of a pseudo-saddle to itself and the last one is the collision of a sliding cycle with a standard saddle.

The last case can already be discarded for the system at hand. The reason for this is the following: The only standard saddle points which a sliding cycle could possibly collide with, are $(0, 0)$ and $(1, 0)$. These points lie on the invariant coordinate axes and hence the only way a sliding cycle could collide with them would be if part of the sliding cycle lies on one of the coordinate axes. Since sliding cycles always contain at least one tangent point and the tangent points have strictly positive components, this is impossible. So there does not exist a collision of a sliding cycle with a standard saddle in this system.

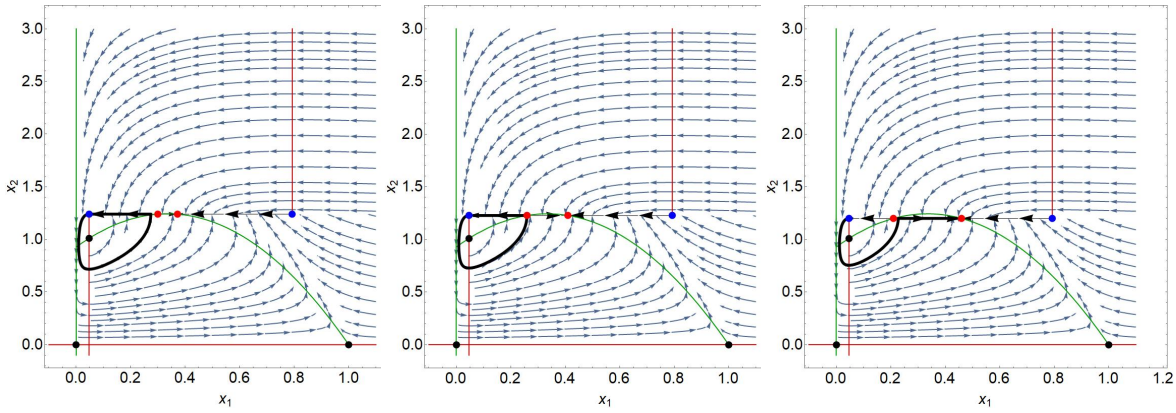

Figure 26: Phase portraits before, at and after the touching bifurcation. The parameter values are $\alpha = 1.24$, $\alpha_0 \approx 1.2275$ and $\alpha = 1.2$ (left to right).

The next thing to check is if there exists a pseudo-homoclinic connection from the pseudo-saddle-node to itself. This can be done numerically by slightly varying α around the value $\alpha_{PSN} \approx 1.2436$ and then comparing where the solution with initial datum set to be T_1 re-enters the sliding segment. The corresponding Matlab code and a more detailed description of the method can be found in appendix B. The numerical analysis shows that when varying α from $\alpha_0 - 0.01$ to $\alpha_0 + 0.01$

with decreasing step size, the solution starting at T_1 always re-enters to the left of the pseudo-saddle(-node). In particular so for $\alpha = \alpha_0$. The re-entry points are continuously depend on the initial condition and hence the findings indicate that there does not exist a pseudo-homoclinic connection from the pseudo-saddle-node to itself.

The last type of pseudo-homoclinic connection that could occur is the connection of a pseudo-saddle to itself. The pseudo-saddle in this system exists for α values roughly between $\alpha = 1.2436$ and $\alpha = 1.0105$ which mark the pseudo-saddle-node bifurcation and the boundary focus bifurcation respectively. It turns out that there exist two such pseudo-homoclinic connections in the system at hand. To detect these, α is varied from $\alpha = 1.2436$ and $\alpha = 1.0105$ with decreasing step size. The re-entry points of the special orbit through T_1 are compared to the location of the pseudo-saddle at each value of α. The re-entry points continuously depend on the initial condition and hence on α. If one can show that for some α_1 and α_2 the re-entry of the special orbit lies to the left of the pseudo-saddle for α_1 and to right for α_2 then there must exists an $\alpha^* \in (\alpha_1, \alpha_2)$ such that the re-entry point of the special orbit coincides with the pseudo-saddle for α^*. So much for the detection part. In order to approximate the α values for which these pseudo-homoclinic connections occur, a method that is based on a bisection scheme is employed. The pseudo-homoclinic connections occur for $\alpha_{HC1} \approx 1.2275$ and $\alpha_{HC2} \approx 1.0294$. The critical phase portraits for these bifurcations are given in figures 26 and 27. The code and short descriptions of the numerical methods employed can be found in appendix B.

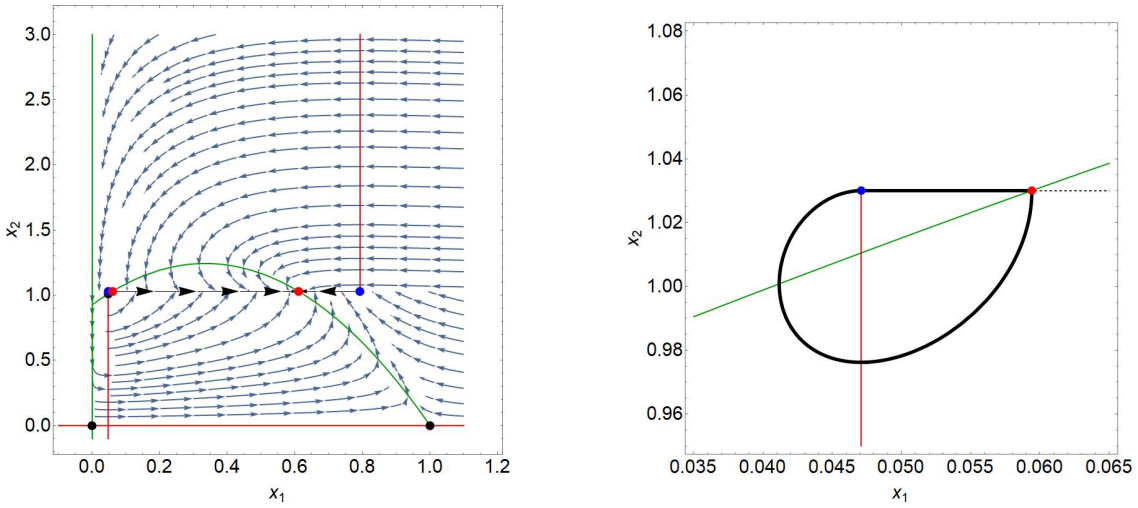

Figure 27: Critical phase portrait for the second pseudo-homoclinic connection at $\alpha \approx 1.0294$. Regular phase portrait and nullclines on the left, zoomed image of the pseudo-saddle on the right.

Pseudo-heteroclinic bifurcations. There are two rather trivial pseudo-heteroclinic connections to be observed. One connects the pseudo-saddle to the pseudo-node for $\alpha \in (\alpha_{PSN}, \alpha_{BF})$. The other one connects the standard saddle $(1, 0)$ to the pseudo-node for $\alpha \in (\alpha_{PSN}, \alpha_{BN})$. These connections can be observed in the earlier presented phase portraits but are only highlighted now for reasons of clarity. The two different connections are illustrated in figure 28. It is interesting to note that for $\alpha \in (\alpha_{HC1}, \alpha_{HC2})$ both branches of the unstable line to the pseudo-saddle connect to the stable pseudo-node.

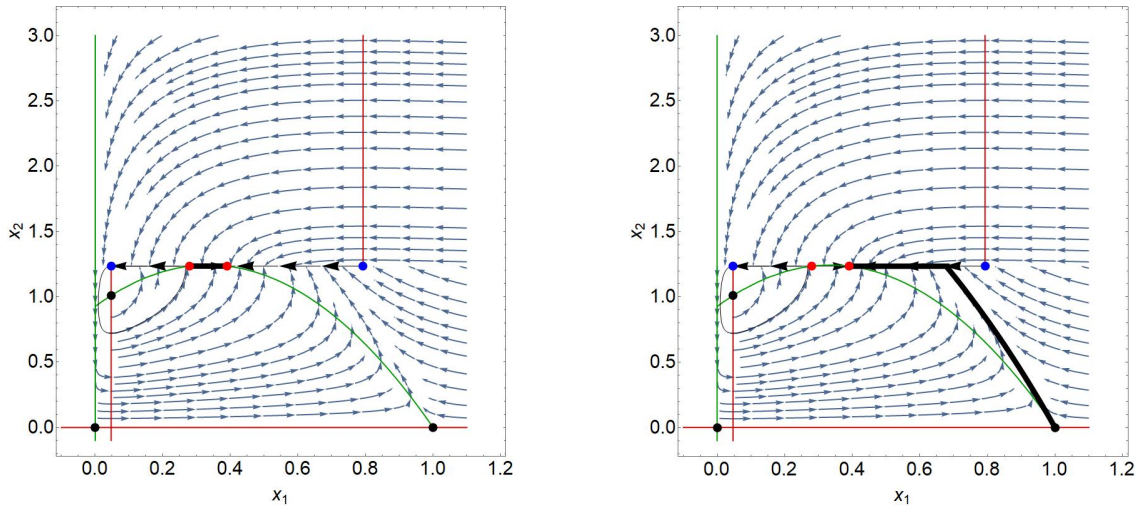

Figure 28: Pseudo-heteroclinic connections for $\alpha = 1.23$. Note that the orbit of the sliding cycle does not contain the pseudo-saddle.

Special orbits never re-enter the sliding segment through a tangent point which excludes behaviour such as buckling or crossing which were briefly touched upon in the end of chapter 4. This concludes the discussion of all global co-dimension one bifurcations that can be observed in this system.

Summary of bifurcations

The table in figure 29 summarizes the bifurcations that occur for $a = 0.3556$, $b = 0.33$, $d = 0.0444$ and $E = 0.2067$ when decreasing α.

α value	local vs. global	bifurcation type
2.4405	global	touching (TC_1)
1.2436	local	pseudo-saddle-node
1.2436	global	sliding heteroclinic connection(s)
1.2275	global	sliding homoclinic connection
1.0294	global	sliding homoclinic connection
1.0105	local	boundary focus (BF_1)
0.6539	local	boundary node (BN_1)

Figure 29: Summary of bifurcations

The critical phase portraits have already been discussed when the bifurcations themselves were presented. To compare the qualitative behaviour before and after these bifurcations, the non critical phase portraits are shown in figures 30 through 33. Depicted are the situations before the touching bifurcation, between each of the listed bifurcations and after the boundary node bifurcation. Note that the pseudo-heteroclinic connections are excluded due to their trivial nature.

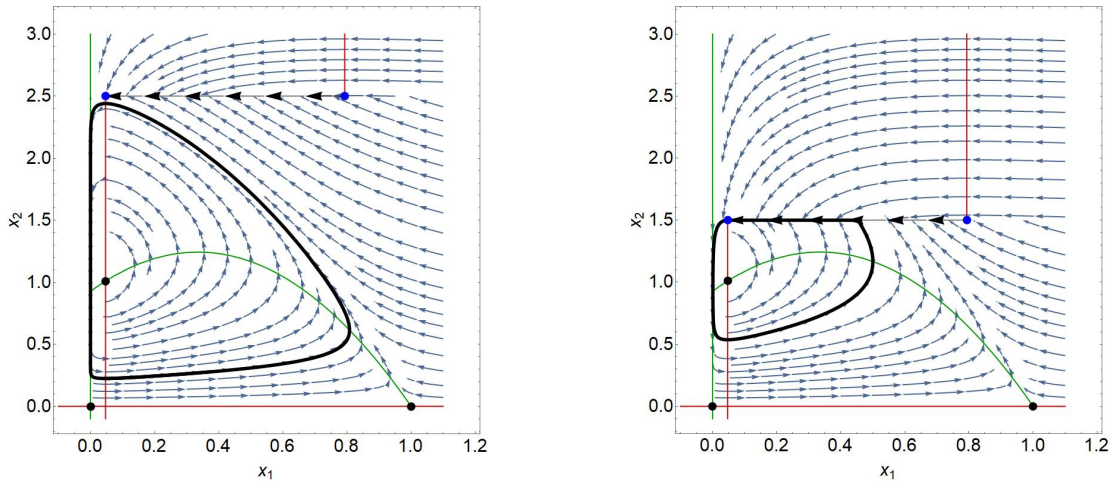

Figure 30: Phase portraits prior to touching bifurcation (left, $\alpha = 2.5$) and prior to pseudo-saddle-node bifurcation (right, $\alpha = 1.5$).

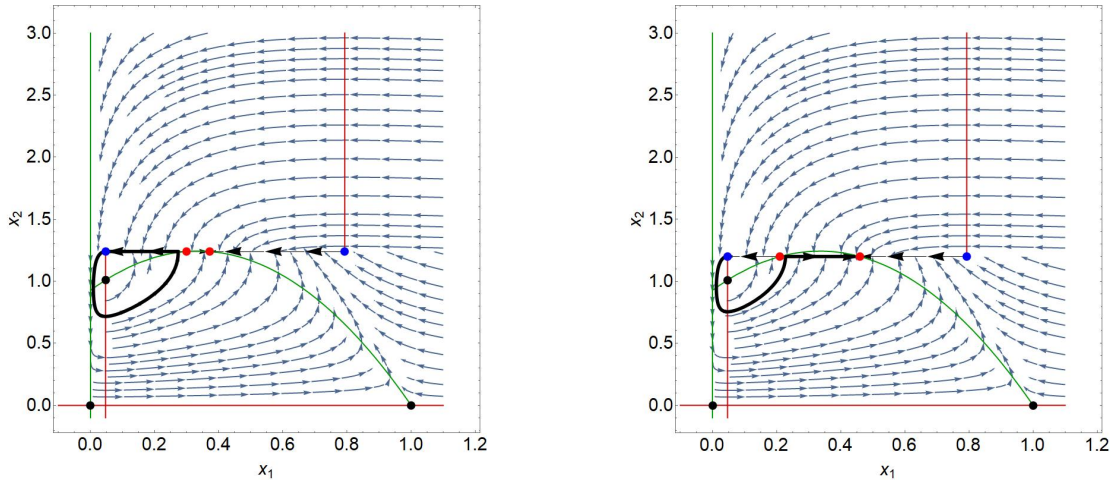

Figure 31: Phase portraits prior to the first pseudo-homoclinic connection (left, $\alpha = 1.24$) and prior to the second pseudo-homoclinic connection (right, $\alpha = 1.02$).

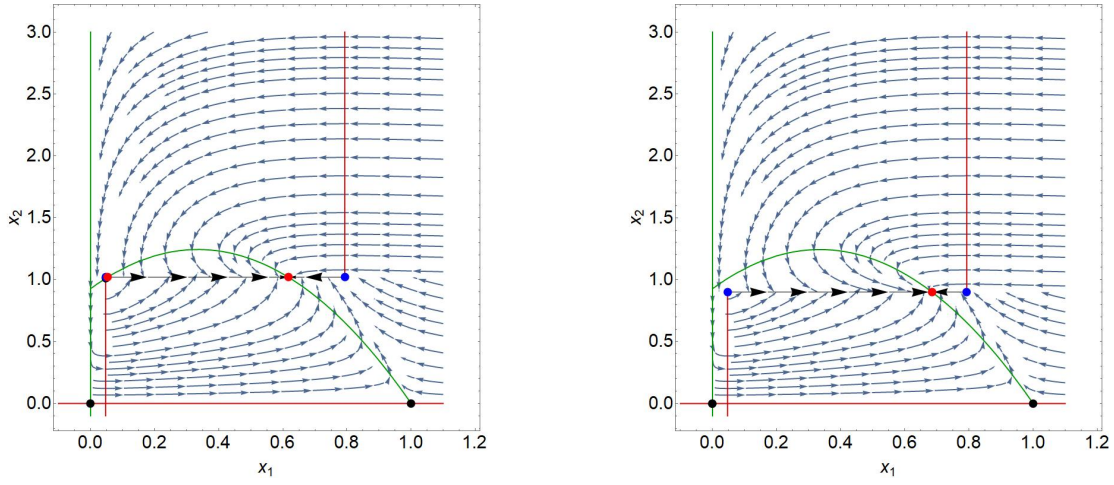

Figure 32: Phase portraits prior to boundary focus bifurcation (left, $\alpha = 1.24$) and prior to boundary node bifurcation (right, $\alpha = 1.02$).

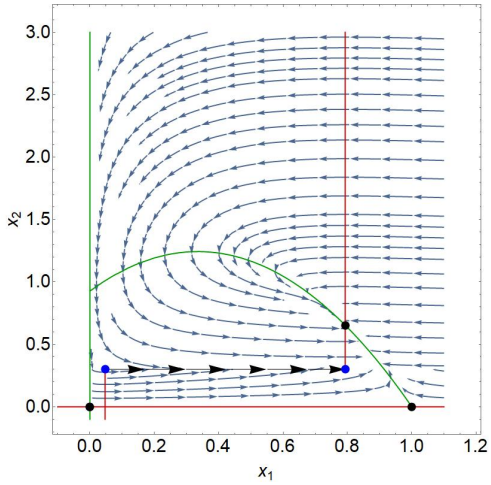

Figure 33: Phase portraits after the boundary node bifurcation ($\alpha = 0.3$).

5.3 Bifurcations for the Case: $\mathbf{b > \frac{a-d}{a+d}}$

To represent the case $b > \frac{a-d}{a+d}$, the parameters are set to $a = 0.3$, $b = 0.4$, $d = 0.15$ and $E = 0.05$.

Local Bifurcations

The key distinction between the case $b > \frac{a-d}{a+d}$ and the case previously discussed is the positioning of the nontrivial x_2-nullcline. The nontrivial x_2-nullcline is still different in the two regions, but now it lies to the right of the maximum of the nontrivial x_1-nullcline in *both* regions. This means that in both regions the coexistence equilibrium is stable and there do not exist any periodic solutions which are completely contained in either S_1 or S_2. To avoid confusion, note that the notation for α_{BF} and α_{BN} is reused and only refers to values for the current parameter setting.

Boundary Focus. As α decreases from a starting value of 2, the first local bifurcation that will occur is the collision of the stable focus with Σ_s. As similarly discussed for the previous case, the value of α that corresponds to the boundary-focus bifurcation is

$$\alpha_{BF} = \frac{b(a - bd - d)}{(a - d)^2} = \frac{8}{5} = 1.6$$

In order to classify this boundary-focus bifurcation it is necessary to observe that a pseudo-equilibrium is born upon collision of the stable focus with Σ_s. As is evident from the phase portrait and the plot of the nullclines in figure 34, the pseudo-equilibrium is a stable pseudo-node. This narrows down the possibilities to BF_3 and BF_4. Taking into account the relative position of the stable focus and the tangent point T_1 to one another eliminates BF_3 as well. The bifurcation is of type BF_4. The local phase portrait can be obtained from the normal form presented in section 4 by reversing all the arrows and reflecting over the vertical axis.

Boundary Node. Exactly analogue to the other parameter setting, there occurs a boundary node bifurcation when the tangent point TP_2 collides with the nontrivial

x_1-nullcline for

$$\alpha_{BN} = \frac{b\,[a - b(d+E) - (d+E)]}{(a-(d+E))^2} = \frac{4}{5} = 0.8.$$

In this case, the matrix representing the linearized system around the coexistence equilibrium in S_2 is

$$J(\bar{x}_1, \bar{x}_2) = \begin{bmatrix} 1 - 2\bar{x}_1 - \frac{ab\bar{x}_2}{(b+\bar{x}_1)^2} & -\frac{a\bar{x}_1}{b+\bar{x}_1} \\ \frac{ab\bar{x}_2}{(b+\bar{x}_1)^2} & 0 \end{bmatrix} = \begin{bmatrix} -\frac{2}{3} & -\frac{1}{5} \\ -\frac{1}{15} & 0 \end{bmatrix}.$$

and has eigenvalues

$$\lambda_1 = -\frac{553}{856} \text{ and } \lambda_2 = -\frac{73}{3537}.$$

which are again both real and negative. So here the coexistence equilibrium is a stable node as well. To answer the question whether the boundary node bifurcation is of type BN_1 or BN_2, note that this bifurcation is due to the collision of the stable pseudo-node that was generated by the boundary focus bifurcation of type BF_4. This means that before and after the boundary node bifurcation there exists a stable (pseudo) equilibrium near the tangent point T_2 and hence the bifurcation must be of type BN_1. The critical phase portraits for the boundary focus bifurcation as well s the boundary node bifurcation are given in figure 34. Similarly to the other parameter configuration, the local phase portrait can be obtained from the BN_1 normal form by considering a reversed order of the images and renaming the regions S_1 and S_2.

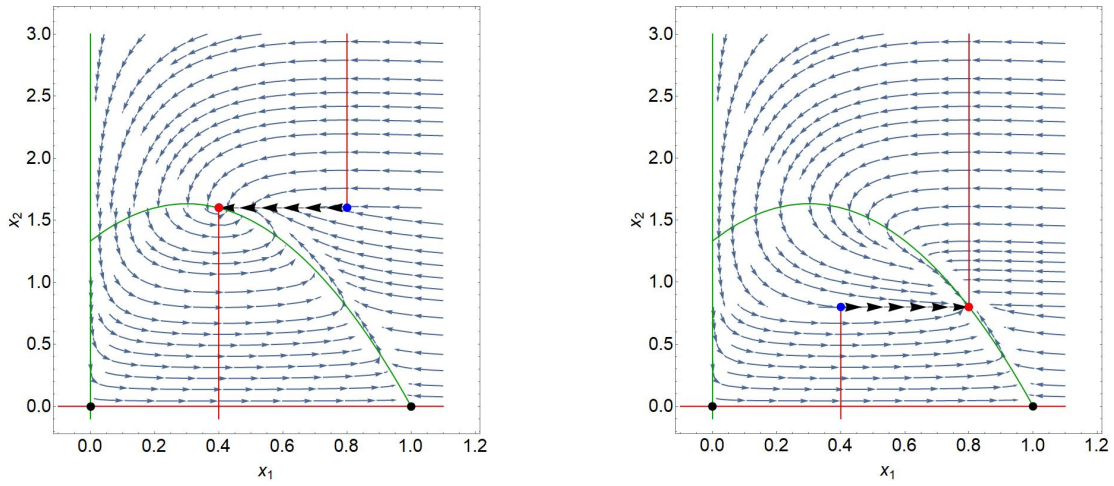

Figure 34: Critical phase portraits for the boundary-focus bifurcation (left, $\alpha = 1.6$) and the boundary-node bifurcation (right, $\alpha = 0.8$).

Global Bifurcations

Neither S_1 nor S_2 can contain any standard periodic solutions. This excludes the possibility of a colliding standard cycle with Σ_s. The analysis of local bifurcations showed that there do not exist any pseudo-saddles nor pseudo-saddle-nodes. Further, following the same argumentation as before, there cannot exist any pseudo-homoclinic connections involving the standard saddles. This means there do not exist any pseudo-homoclinic bifurcations. Since there is only one sink present for $\alpha > 0$, it is obvious

that for α-values after the boundary focus bifurcation and before the boundary node bifurcation there exists a pseudo-heteroclinic connection from the saddle $(1, 0)$ to the stable pseudo-node. This pseudo-heteroclinic connection is illustrated in figure 35. It is to be pointed out that there cannot exist any buckling or crossing. This is because any orbit that enters the sliding segment approaches the pseudo-node eventually and stays there. For $\alpha \notin [\alpha_{BN}, \alpha_{BF}]$ any solution will approach the sink immediately after it left Σ_s through T_1 or T_2. Hence there do not occur any kinds of global bifurcations involving buckling or crossing.

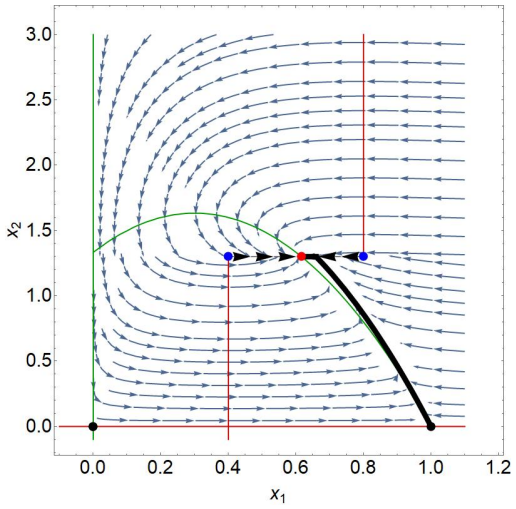

Figure 35: Phase portraits depicting a pseudo-heteroclinic connection for $\alpha = 1.3$.

Summary of bifurcations

The table in figure 36 summarizes the bifurcations that occur for $a = 0.3$, $b = 0.4$, $d = 0.15$ and $E = 0.05$ when decreasing α.

α value	local vs. global	bifurcation type
1.6	local	boundary focus (BF_4)
1.6	global	sliding heteroclinic connection
0.8	local	boundary node (BN_1)

Figure 36: Summary of bifurcations

Similar to the procedure before, the non critical phase portraits are shown in figures 37 and 38. Depicted are the situations before and after the boundary focus bifurcation as well as the situation after the boundary node bifurcation. Again, the pseudo-heteroclinic connections are excluded due to their trivial nature.

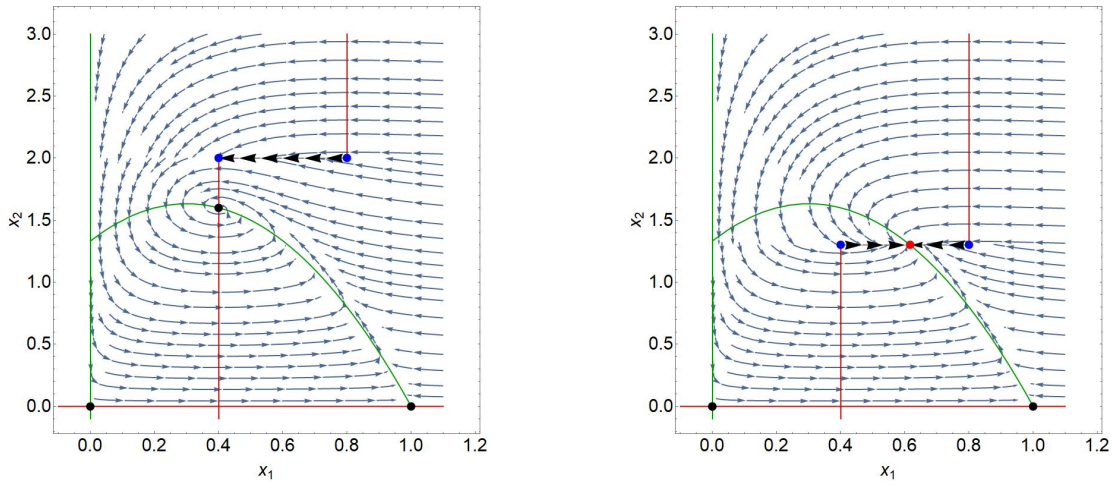

Figure 37: Phase portraits prior to boundary focus bifurcation (left, $\alpha = 2$) and prior to boundary node bifurcation (right, $\alpha = 1.3$).

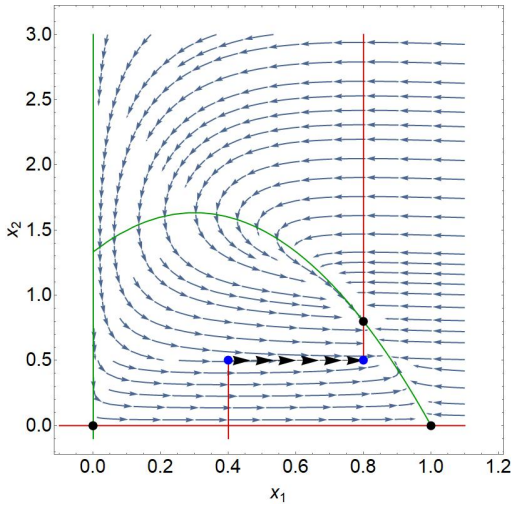

Figure 38: Phase portraits after the boundary node bifurcation ($\alpha = 0.5$).

5.4 Conclusion of Results

In this chapter, we have seen how the theory of Filippov systems and DIBs can be applied to a modified version of the Rosenzweig-Macarthur model with population dependent harvesting of the predators. Overall the introduction of harvesting when $x_2 > \alpha$ had a profound impact on the behaviour of solutions in the two cases treated. However, it is fair to say that the effect of this change is far more drastic for the parameter setting where a periodic orbit is present in region S_1 so for $b < \frac{a-d}{a+d}$. In the case where there is no periodic orbit present ($b > \frac{a-d}{a+d}$), the behaviour of solutions for the Filippov system is very similar to that of solutions to the continuous system one gets by extending $f^{(1)}$ or $f^{(2)}$ to the entire first quadrant. For both systems there is a single (pseudo-)equilibrium present which attracts all solutions in the interior of the first quadrant. Varying α in the Filippov system in this case merely changes the way how these solutions approach the equilibrium.

On the other hand, in the setting $b < \frac{a-d}{a+d}$, for large α a periodic orbit is present in region S_1 which is attracting all solutions in the interior of the first quadrant

which are not the coexistence equilibrium. As α is varied the periodic orbit becomes a sliding orbit and for the interval of α values between the pseudo-saddle-node bifurcation and the first pseudo-homoclinic orbit, there are two attractors present in the system. The first one is the stable sliding cycle and the second one is the stable pseudo-node which was generated in the pseudo-saddle-node bifurcation. This is a remarkable result when one considers that a state featuring multiple attractors is simply impossible for the continuous version of the Rosenzweig-MacArthur model. Another interesting event is the disappearance of the sliding cycle in the first pseudo-homoclinic bifurcation. Here, the sliding cycle disappears only to reappear in the second pseudo-homoclinic bifurcation. For α values between the first and second pseudo-homoclinic bifurcation there is again only one attractor present. This means in summary that when lowering α from 2.5, the system goes from having a single attractor (standard cycle) to two attractors to a single attractor to two attractors and finally to a single attractor. Finally, it is to be noted that the results for the bifurcation analysis, i.e. the detection of bifurcations as well as the approximation of critical α values, agrees to a large extend to the findings by Kuznetsov et. al. [8]. Very small deviations of results are very likely due to a difference in numerical approximation procedures.

6 Discussion

The aim of this thesis was to explore the effect that population dependent harvesting in a modified version of the Rosenzweig-MacArthur predator-prey model, has on the global behaviour of solutions describing interspecies-interactions. Necessary theory on Filippov systems and discontinuity-induced bifurcations was presented and applied to the model. In doing so, a number of results and findings published in the article by Kuznetsov et. al. [8] have been replicated and verified. The main surprise is that upon introduction of population dependent harvesting, the predator-prey model can now have multiple attractors which is impossible in the case of a continuous Rosenzweig-MacArthur model.

In a real life setting, adjusting the value of α is the control we can exert on an ecological model like this. Imagine an ecological system in which the population dynamics can be approximated by the continuous Rosenzweig-MacArthur model. Further assume that there exists a periodic solution which lies relatively close to the coordinate axes. With a bit of bad timing of some kind of external perturbation like extreme weather conditions or the interference of another species, one of the populations described might get very close to the brink of extinction. To avoid the formation of such sensible periodic population dynamics, fine-tuned dynamic adjustment of population-density-dependent harvesting could be introduced. This could lead to the stabilization of these population densities around a periodic sliding cycle with excursions that do not lie so close to any of the coordinate axes. Alternatively, the population densities might stabilize around a pseudo-equilibrium which would not be present in the absence of harvesting.

Biological and ecological applications as presented in this thesis are not the only field that Filippov systems find application in. Further applications include the modeling of mechanical systems involving dry friction as treated in articles [2] and [7], or the modeling of control systems with switching control laws as for example article [1] and [3].

Lastly, a few words on the limitations of this thesis and where to go next. The numerical methods employed in this thesis are implemented in a rather naive way and bear room for improvement when it comes to efficiency. At the same time the produced results almost perfectly agree with the findings by Kuznetsov et. al. [8] and match the theoretic predications. Having discussed so many properties of planar Filippov systems, it would only be natural to investigate the question whether chaos can arise in these systems. Due to time limitations, this question could unfortunately not be addressed. This thesis is focused on the bifurcation analysis with respect to single parameter. A logical next step would be to strive for a complete analysis with respect to all system parameters. This would require a much more advanced repertoire of analytical and numerical tools compared to what has been used throughout this text. Another direction to take could be to investigate one parameter families of Filippov systems of higher dimension. The classification of co-dimension one bifurcations for three-dimensional Filippov systems is already much more complex than the one for planar systems and seems unfeasible to attempt at the moment, but with the development of more sophisticated analytic methods this might be a next milestone in the study of Filippov systems.

References

[1] G. Bartolini, F. Parodi, V. Utkin, and T. Zolezzi. The simplex method for nonlinear sliding mode control. *Mathematical Problems in Engineering*, 4(6):461–487, 1999.

[2] J. B. Biemond, N. van de Wouw, and H. Nijmeijer. Bifurcations of equilibrium sets in mechanical systems with dry friction. *Physica D: Nonlinear Phenomena*, 241(22):1882–1894, 2012.

[3] F. Della Rossa and F. Dercole. The transition from persistence to nonsmooth-fold scenarios in relay control system. In *Proceedings of the 18th IFAC World Congress, Milano*, 2011.

[4] M. Di Bernardo, C. J. Budd, A. R. Champneys, P. Kowalczyk, A. B. Nordmark, G. O. Tost, and P. T. Piiroinen. Bifurcations in nonsmooth dynamical systems. *SIAM review*, 50(4):629–701, 2008.

[5] A. F. Filippov. *Differential Equations with Discontinuous Righthand Sides: control systems*, volume 18. Springer Science & Business Media, 2013.

[6] M. W. Hirsch, S. Smale, and R. L. Devaney. *Differential Equations, Dynamical Systems, and an Introduction to Chaos*. Academic press, 2012.

[7] P. Kowalczyk and P. Piiroinen. Two-parameter sliding bifurcations of periodic solutions in a dry-friction oscillator. *Physica D: Nonlinear Phenomena*, 237(8):1053–1073, 2008.

[8] Y. A. Kuznetsov, S. Rinaldi, and A. Gragnani. One-parameter bifurcations in planar filippov systems. *International Journal of Bifurcation and chaos*, 13(08):2157–2188, 2003.

[9] X. Liu. *The discontinuous Hopf-transversal system and its geometric regularization*. [Sn], 2013.

[10] H. L. Smith. The Rosenzweig-Macarthur predator-prey model. *School of Mathematical and Statistical Sciences, Arizona State University: Phoenix*, 2008.

[11] P. Turchin. *Complex Population Dynamics: A theoretical/empirical synthesis*, volume 35. Princeton university press, 2003.

A Appendix: Concepts in Dynamical Systems

In this first appendix, some basic concepts from complex dynamical systems theory will be briefly introduced. These topics are the trace-determinant plane for planar systems, flow-boxes and flow-box coordinates, and finally the Poincaré map. The material for this appendix was largely taken from the book *Differential Equations, Dynamical Systems and an Introduction to Chaos* by Devaney et. al. [6]. The sections in the book are chapter 4 and 10.

A.1 The trace-determinant plane

For a planar linear autonomous system

$$\dot{\boldsymbol{x}} = A\boldsymbol{x} = \begin{bmatrix} a & b \\ c & d \end{bmatrix} \boldsymbol{x},$$

the stability of an equilibrium and the behaviour of the system around this equilibrium, is entirely encoded in the eigenvalues and eigenvectors of the system matrix A. The eigenvalues of A are given by the solutions to the characteristic equation

$$\lambda^2 - (a+d)\lambda + (ad - bc) = 0.$$

Note that this can be rewritten in terms of the trace and the determinant of A as follows

$$\lambda^2 - tr(A)\lambda + det(A) = 0.$$

If we denote $tr(A)$ by T and $det(A)$ by D, then the eigenvalues are given by

$$\lambda_{1,2} = \frac{1}{2}\Big(T \pm \sqrt{T^2 - 4D}\Big). \tag{13}$$

Now we know how the eigenvalues depend on the trace and the determinant. It follows from equation (13) that the eigenvalues are real and coincide if $T^2 = 4D$. Further, the eigenvalues are

(A) *real*, *distinct* and

- (i) have opposite sign if $T^2 > 4D$ and $D < 0$,
- (ii) are negative if $T < 0$ and $T^2 > 4D$,
- (iii) are positive if $T > 0$ and $T^2 > 4D$,

(B) *complex conjugates* with

- (i) positive real part and nonzero imaginary part if $T > 0$ and $T^2 < 4D$,
- (ii) negative real part and nonzero imaginary part if $T < 0$ and $T^2 < 4D$,
- (iii) zero real part if $T = 0$ and $T^2 < 4D$.

The location of the tuple (T, D) in the plane relative to the parabola $T^2 = 4D$ and the coordinate axes yields all the relevant information to describe the system behviour. How the trace and determinant relate to the phase portraits of a system is summarized in figure 39.

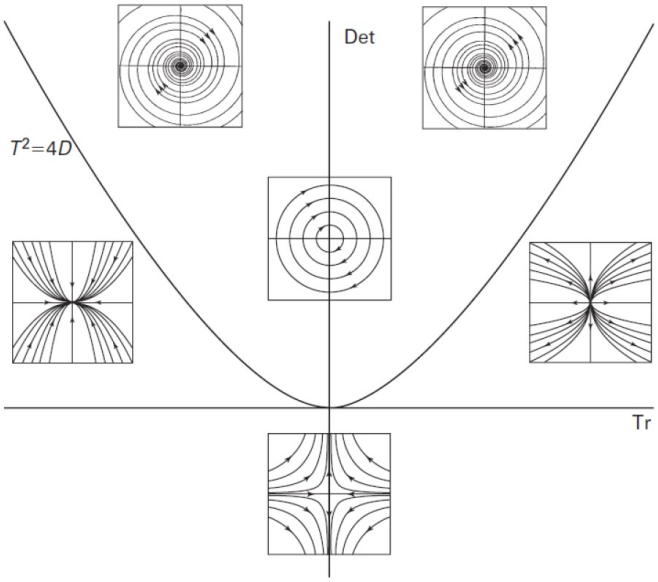

Figure 39: Dependence of stability on trace and determinant. Source: Devaney et. al. [6]

A.2 Flow-Box Coordinates

In chapter 4 it is assumed that the vector field $f^{(2)}(\boldsymbol{x})$ can be considered to be orthogonal to the discontinuity boundary Σ in a neighborhood of a point $\boldsymbol{X}_0$ on Σ where $f^{(2)}(\boldsymbol{X}_0) \neq 0$. This greatly simplifies the following analysis of discontinuity induced bifurcations. The fact that we can assume $f^{(2)}(\boldsymbol{x})$ to be locally orthogonal to Σ can be derived by constructing what is called a *flow-box* around $\boldsymbol{X}_0$. Once a flow box has been constructed it is possible to introduce convenient coordinates within the flow box.

Constructing the Flow Box

In general the first step in constructing a flow box is to define what is called the *transverse line* at $\boldsymbol{X}_0$. This is the straight line through $\boldsymbol{X}_0$ which is perpendicular to $f^{(2)}(\boldsymbol{X}_0)$. The transverse line $l(\boldsymbol{X}_0)$ is parametrized by a function $h : \mathbb{R} \to l(\boldsymbol{X}_0)$ which is given by

$$h(u) = \boldsymbol{X}_0 + u\boldsymbol{V}_0.$$

Here, $\boldsymbol{V}_0$ is a vector of unit length, based at $\boldsymbol{X}_0$ and perpendicular to $f^{(2)}(\boldsymbol{X}_0)$, so $\boldsymbol{V}_0$ lies along $l(\boldsymbol{X}_0)$. This means that at $\boldsymbol{X}_0$, the transverse line $l(\boldsymbol{X}_0)$ is perpendicular to $f^{(2)}(\boldsymbol{X}_0)$ and by the continuity of $f^{(2)}$, there must exists an open interval $\mathcal{S}$ on $l(\boldsymbol{X}_0)$ surrounding $\boldsymbol{X}_0$ such that $f^{(2)}(\boldsymbol{x})$ is **not** tangent to $l(\boldsymbol{X}_0)$. Such an open interval on $l(\boldsymbol{X}_0)$ is called a *local section* at $\boldsymbol{X}_0$. On a local section $\mathcal{S}$, the vector field $f^{(2)}(\boldsymbol{x})$ does not vanish.

Let $\mathcal{N} \subset \mathbb{R}^2$ be a neighborhood containing the origin. Denote ϕ as the flow associated with the differential equation $\dot{\boldsymbol{x}} = f^{(2)}(\boldsymbol{x})$. The next step is to define a map Ψ which maps $\mathcal{N}$ to a neighborhood of $\boldsymbol{X}_0$ in the following way:

$$\Psi(s, u) = \phi_s(h(u))$$

The image of the vertical line $(0, u) \in \mathcal{N}$ under the mapping Ψ is the local section $\mathcal{S}$ itself. Further, under Ψ, horizontal lines in $\mathcal{N}$ get mapped to pieces of solution

curves of the system at hand. Choosing $\mathcal{N}$ sufficiently small, the map Ψ becomes one-to-one. The image $\Psi(\mathcal{N})$ is called the flow box at $\boldsymbol{X}_0$. Now how does this apply to our problem?

Consider a non-equilibrium point $\boldsymbol{X}_0$ of $f^{(2)}(\boldsymbol{x})$ for which $f^{(2)}(\boldsymbol{X}_0)$ is transversal to Σ. Let $\gamma : \mathbb{R} \to \Sigma \subset \mathbb{R}^2$ be a smooth parametrization of Σ such that $\gamma(0) = \boldsymbol{X}_0$. Further, let $y_2 = H(\boldsymbol{x}, \alpha)$. Now let $\boldsymbol{Z}_0$ be an arbitrary point in the flow box at $\boldsymbol{X}_0$, then $\boldsymbol{Z}_0$ can be expressed in terms of the new coordinates y_1 and y_2, where y_1 is the intersection of Σ and the orbit in S_2 through $\boldsymbol{Z}_0$, while $y_2 = H(\boldsymbol{Z}_0, \alpha)$. In these new coordinates, Σ is given by $y_2 = 0$ and the orbits of $f^{(2)}$ are given by $y_1 = const.$. The mapping $x \mapsto y$ is a local diffeomorphism. This is true since for sufficiently small $\mathcal{N}$, Ψ is one-to-one and smooth. This change of coordinates is justification to locally consider $f^{(2)}(x, \alpha)$ to be orthogonal to Σ.

A.3 The Poincaré Map

The Poincaré Map is a useful construction that can be employed to determine whether a periodic orbit is asymptotically stable or not. Consider a periodic orbit γ for some planar system. Let X_0 be a point on γ and let $\mathcal{S}$ be a local section at X_0. The Poincaré Map associated to γ is then defines as

$$P(X) = \phi_t(X)$$

where t is the smallest positive time such that $\phi_t(X) \in \mathcal{S}$. So we consider the first return back to the local section $\mathcal{S}$. Note that P need not be defined on all of $\mathcal{S}$ as certain points on the local section could very well never return back to it. However, we know that

$$P(X_0) = X_0$$

since $X_0 \in \gamma$. The Implicit Function Theorem implies then that there exists some neighborhood of X_0 for which P is well defined and continuously differentiable.

Theorem. *Let $X' = F(X)$ be a planar system and assume that $X_0 \in \gamma$, where γ is a periodic orbit. Let P be a Poincaré map defined in a neighborhood of X_0 in some local section. If $|P'(X_0)| < 1$, then γ is asymptotically stable.*

Proof. Let $X' = F(X)$ be a planar system and $X_0 \in \gamma$, where γ is a periodic orbit of the system $X' = F(X)$. Let $\mathcal{S}$ be a local section at X_0 and construct a Poincaré Map as described above. For planar systems, local sections $\mathcal{S}$ are subsets of straight lines through X_0. Under a diffeomorphic change of coordinates, we may regard $\mathcal{S}$ as a subset of $\mathbb{R}$ such that $X_0 = 0$. This means that P can be seen as a function $P : \mathbb{R} \to \mathbb{R}$ such that $P(0) = 0$. If $P'(0) < 1$, P takes the form

$$P = ax + \text{higher-order-terms}, \ |a| < 1$$

This means that for x close to 0, $P(x)$ is even closer to 0. It follows that each time a solution, which is already sufficiently close to γ, returns to $\mathcal{S}$, the returning points get closer and closer to X_0. It follows that γ is asymptotically stable. □

B Appendix: Matlab Code

This appendix summarizes the numerical tools and methods that are needed in the bifurcation analysis for the modified Rosenzweig-Macarthur model. All necessary simulations and calculations were done using Matlab. In the following, a short description of the function or script and its purpose will be discussed, then the code is presented. The calculations in this appendix are executed on a computer with a Windows 10 operating system and the version of Matlab in use is MatlabR2018a. The processor is an AMD FX8320E Eight-Core, 3.20 GHz and the computer has 8.00 GB of installed RAM.

ODE45 solver

Matlab has a build-in function called *ode45* which can be used to solve systems of ordinary differential equations. The syntax for this solver is as follows

$$[t, y] = ode45(odefun, tspan, y0, options).$$

The first input is some function(handle) *odefun* which represents the right-hand side of the system of differential equations we wish to integrate. The input *tspan* indicates the timespan over which we integrate. The vector *y0* is a set of initial conditions and *options* contains more advanced options such as setting the relative tolerance used to limit the local discretization errors. The outputs are t which is just *tspan* and the vector y. The rows of y contain the x_1 and x_2-coordinates of the points that are the numerical approximation of the solution curve to the vector field described by *odefun* with initial condition *y0*. To estimate the solution, ode45 computes an approximate solution and a corresponding error estimate using Runge-Kutta methods of orders 4 and 5. The relative error made at each individual step can be set to a certain level and the solver will adaptively adjust its step-size to match the indicated error. Of course this is only possible to a certain degree and the relative error is set to 10^{-12}. The criterion for the selection of this tolerance was the intention to increase the precision as much as possible without having a runtime that exceeds one minute. This is a very subjective decision which also depends on the computational facilities available but in any case the level of precision is sufficient for the purposes of this thesis.

Vector field $f^{(1)}$

The function titled *funS1* as shown in figure 40 is the implementation of the vector field $f^{(1)}(x)$. The parameters a, b, d and E are passed to the function using the vector *par*. Note that d (respectively $d + E$) are represented by the variable *he* and are determined externally, so not within this function but in a script calling this function. The variable t is not used but needs to be stated as input in order to be able to use this function with Matlab's *ode45* solver. Finally, the variable *xin* is a vector containing x_1 and x_2. Similarly so for *xout*.

```
function [xout] = funS1(t,xin,par)
a=par(1);
b=par(2);
he=par(3);
xout=zeros(2,1);
xout(1)=xin(1)*(1-xin(1))-(a*xin(1)*xin(2))/(b+xin(1));
xout(2)=(a*xin(1)*xin(2))/(b+xin(1))-he*xin(2);
end
```

Figure 40: The vector field $f^{(1)}$.

Linearization of $f^{(1)}$ around the unstable focus in S_1

The function titled *funlinS1* as shown in figure 41 is the implementation of the linearization of $f^{(1)}$ around the unstable focus in S_1. The descriptions for inputs and outputs are analogue to the ones for *funS1*.

```
function [xout] = funlinS1(t,xin,par)
%linearized system around the unstable focus in S1
a=par(1);
b=par(2);
he=par(3);
xout=zeros(2,1);
xout(1)=-((he*(a*b-a+b*he+he))/(a*(a-he)))*xin(1)-he*xin(2);
xout(2)=(a-b*he-he)/(a)*xin(1);
end
```

Figure 41: The linearization of the vector field $f^{(1)}$ around the unstable focus in S_1.

Function to find crossing

The function titled *findCrossAlpha* as shown in figure 42 solves the problem of finding the x_1-location of the point where an orbit through T_1 re-enters into the sliding segment. It takes as input a matrix y and a scalar α. The vector y is the output of the build-in *ode45* solver. In our case, y is a $k \times 2$ matrix, where k is the number of rows of y. This function loops over the size of the vector y and at each iteration checks if the x_2-coordinate is larger than α. If at the i-th iteration the x_2-coordinate is larger than α then this means that the sliding segment has been crossed and the x_1-location of the intersection is approximated using the last two iterates. If the solution represented by y should not cross the sliding segment at all, then an error message is displayed.

Boundary Focus

We consider the linearization of the vector field $f^{(1)}$ around the focus equilibrium in the region S_1. The script in figure 43 is used to calculate where the orbit starting at $(-\frac{d}{c}, 1)$ returns to the line of constant $x_2 = 1$ relative to the point $(-\frac{b}{a}, 1)$. To do so, various parameters and variables are initialized, the solution starting at $(-\frac{d}{c}, 1)$

```
function [xintersect] = findCrossAlpha(y,alpha)
    for i=1:size(y)
        if alpha-y(i,2)<0
            xintersect=(y(i,1)+y(i-1,1))/2;
            break
        else
            xintersect=0;
        end
    end
    if xintersect==0
        disp('error in crossing')
    end
end
```

Figure 42: The function used to determine the x_1-location of the re-entry point.

is computed numerically and its re-entry point to the line $x_2 = 1$ is determined. Depending on the location of re-entry, the script displays text on screen indicating where this re-entry lies relative to the point $(-\frac{b}{a}, 1)$. The script indicates that the re-entry lies to the left of the point $(-\frac{b}{a}, 1)$. In the context of the discussion in chapter 5.2, this implies that the boundary-focus bifurcation is of type BF_1.

```
clear all
%parameters
a=0.3556;
b=0.33;
d=0.0444;
%store parameters in vector to pass to ode45
par(1)=a;
par(2)=b;
par(3)=d;
%parameters in linearized system
la=-(d*(a*b-a+b*d+d))/(a*(a-d));
lb=-d;
lc=(a-b*d-d)/(a);
ld=0;
%relevant points
P1=[-ld/lc,1];
P2=[-lb/la,1];
%solve the ode
opts = odeset('RelTol',1e-12);
tspan=0:0.001:30;
y0=P1;
[t,y]=ode45(@(t,y)funlinS1(t,y,par),tspan,y0,opts);
%compute re-entry x-location and compare
xcross=findCrossAlpha(y,1);
if xcross<P2(1)
    disp('Re-entry lies on the left');
elseif xcross>P2(1)
    disp('Re-entry lies on the right');
else
    disp('Coincidence or error');
end
```

Figure 43: The script used to distinct the bifurcation type BF_1 from BF_2.

Touching bifurcation approximating α_0

The intention of this procedure is to approximate the value of α for which the touching bifurcation occurs. The corresponding script is shown in figure 44. By inspection of the corresponding phase portrait, the initial condition is picked close to the periodic orbit. The idea is to execute two approximations to the periodic orbit. The first approximation aims to find a point which lies close to the periodic. The second approximation has a smaller step-size and from its output the point on the periodic orbit with the largest x_2 value will be approximated. The approximation yields that $\alpha_0 \approx 2.4405$.

```
clear all
%parameters
a=0.3556;
b=0.33;
d=0.0444;
Ee=0.2067;
alpha=1.2;
%store parameters in vector to pass to ode45
par(1)=a;
par(2)=b;
par(3)=d;
par(4)=Ee;
%construct initial solution to approximate periodic orbit
tspan=0:1:1000;
y0=[0.4,2];
opts = odeset('RelTol',1e-12);
[tapprox,yapprox]=ode45(@(t,y)funS1(t,y,par),tspan,y0,opts);
%construct final approximation based on initial conition from ...
    previous one
tspan=0:0.001:75;
y1=[yapprox(end,1),yapprox(end,2)];
opts = odeset('RelTol',1e-12);
[t,y]=ode45(@(t,y)funS1(t,y,par),tspan,y1,opts);
%find maximum value in periodic orbit
alphacrit=max(y(:,2))
```

Figure 44: Script used to approximate the value of α at the touching bifurcation.

Pseudo-saddle-node Homoclinic connection

The purpose of the script in figure 45 is to show that there does not exist a pseudo-homoclinic connection from the pseudo-saddle-node to itself for the $\alpha_0 = 1.2436$. In order to do that α is varied from $\alpha_0 - 0.01$ to $\alpha_0 + 0.01$ with a step-size of 0.0002. This is to account for imprecisions in the calculation of α_0. At each iteration the solution starting at T_1 is computed and the point at which the solution re-enters the sliding segment is compared to the location of the pseudo-saddle(-node). The output is a column vector that indicates in text whether the re-entry point lies to left or to the right of the pseudo-saddle(-node). The output vector consists of only "left" and "left$*$" entires. Since the solutions are continuously depend on α, this indicates that the orbit starting at T_1 returns to the left of the pseudo-saddle-node and hence there does not exist a pseudo-homoclinic connection for $\alpha_0 = 1.2436$.

```
clear all
%parameters
a=0.3556;
b=0.33;
d=0.0444;
Ee=0.2067;
%exact value of bifurcation
alphaPSN=(b+1)^2/(4*a);
%store parameters in vector to pass to ode45
par(1)=a;
par(2)=b;
par(3)=d;
par(4)=Ee;
%Analysis with main loop
nloop=100;
xcross=zeros(1,nloop);
text=strings(1,nloop);
opts = odeset('RelTol',1e-12);
for i=1:nloop+1
    %loop parameters
    epsi=0.02/nloop;
    alpha=alphaPSN-0.01+epsi*(i-1);
    %tangent point
    TP1=[(b*d)/(a - d), alpha];
    %find pseudo-equilibria
    SigDynamPoly = [1 b-1 a*alpha-b];
    roots1 = roots(SigDynamPoly);
    EqSig2=[roots1(1),alpha];
    EqSig3=[roots1(2),alpha];
    %solve the ode
    tspan=0:0.001:40;
    y0=TP1;
    [t,y]=ode45(@(t,y)funS1(t,y,par),tspan,y0,opts);
    %compute re-entry x-location
    xcross(i)=findCrossAlpha(y,alpha);
    %compare re-entry point to location of pseudo-saddle-node
    %check if solution crosses Sigma
    if xcross(i)≥ 0
        %check if alpha is sub/super-critial
        if isreal(EqSig3)==true
            %compare re-entry point to location of pseudo-saddle
            if (EqSig3(1)-xcross(i))>0
                text{i}='Left';
            elseif (EqSig3(1)-xcross(i))==0
                text{i}='0';
            else
                text{i}='Right';
            end
        else
            %compare re-entry point to location of pseudo-saddle-node
            if ((1-b)/2-xcross(i))>0
                text{i}='Left*';
            elseif ((1-b)/2-xcross(i))==0
                text{i}='0*';
            else
                text{i}='Right*';
            end
        end
    else
        text{i}='error';
    end
end
text'
```

Figure 45: Script pseudo-saddle-node

Pseudo-saddle homoclinic connections

The purpose of the script in figure 46 is to show that there exist two pseudo-homoclinic connections from the pseudo-saddle to itself when varying α. Moreover, the α-values for which the pseudo-homoclinic connections occur will be approximated by using the script in figure 47. The structure of these scripts is very similar to the script that is used to detect pseudo-homoclinic connections for the pseudo-saddle-node. The key difference is that α is varied from α_{PSN} to α_{BF} with a step size of with a step size

$$\Delta\alpha = \frac{\alpha_{PSN} - \alpha_{BF}}{50} \approx 0.0047.$$

At each iteration the solution starting at the tangent point T_1 is approximated and it is compared where this solution returns to the sliding segment relative to the position of the pseudo-saddle. If the return point lies to the left of the pseudo-saddle for iteration i then the word "left" is stored in the i-th entry of the output vector *text*. Similarly so for the situation if the return point lies to the right of the pseudo-saddle. If the return point and the pseudo-saddle coincide, "0" will be stored in the corresponding entry. All entries of the vector read "right" except for the first 4 and the last 5 entires. This indicates that there are two pseudo-homoclinic connections as there are two α intervals in which the return point clearly changes from one side of the pseudo-saddle to the other. By continuous dependence of initial conditions, there must be two pseudo-homoclinic connections.

The next step is now to approximate these critical α values. To approximate these values, the script in figure 47 is used. An initial α above the critical value is determined by inspection. Then α is decreased with an initial step-size of $\Delta\alpha = 10^{-1}$ and in each iteration the relative position of the return point and the pseudo-saddle are compared. Whenever the return point changes in a single iteration from the left side to the right side of the pseudo-saddle, the step-size is halved and we start to add $\Delta\alpha$ instead of subtracting it. Exactly analogue: Whenever the return point changes in a single iteration from the right side to the left side of the pseudo-saddle, the step-size is halved and $\Delta\alpha$ is subtracted again. This yields a bisective scheme which induces a convergence of the α-values to the critical α-value for which the first pseudo-homoclinic connections occurs. The first pseudo-homoclinic connection occurs for $\alpha_0 \approx 1.2275$.

The same script in figure 47 can be used to approximate the critical α-value for the second pseudo-homoclinic connection as well under the implementation of minor changes. The necessary changes are

1. alpha=1.24 $\rightarrow$ alpha=1.04 (line 17),
2. eps=10^{-1} $\rightarrow$ eps=10^{-3} (line 19),
3. sign= 1 $\rightarrow$ sign= -1 (line 45),
4. sign= -1 $\rightarrow$ sign= 1 (line 49).

The changes account for the different position of the pseudo-equilibrium relative to the tangent point T_1 and the returning points of the orbits through T_1. The second pseudo-homoclinic connection occurs for $\alpha_0 \approx 1.0294$.

```
clear all
%parameters
a=0.3556;
b=0.33;
d=0.0444;
Ee=0.2067;
%exact values of bifurcation
alphaPSN=(b+1)^2/(4*a);
alphaBF=b*(a-b*d-d)/((a-d)^2);
%store parameters in vector to pass to ode45
par(1)=a;
par(2)=b;
par(3)=d;
par(4)=Ee;
%detection of pseudo-homoclinic orbits
nloop=50;
xcross=zeros(1,nloop);
text=strings(1,nloop);
opts = odeset('RelTol',1e-12);
for i=1:nloop+1
    %loop parameter
    epsi=(alphaPSN-alphaBF)/nloop;
    alpha=alphaPSN-epsi*(i-1);
    %tangent points
    TP1=[(b*d)/(a - d), alpha];
    %find pseudo-equilibria
    SigDynamPoly = [1 b-1 a*alpha-b];
    roots1 = roots(SigDynamPoly);
    EqSig3=[roots1(2),alpha];
    %solve the ode
    tspan=0:0.001:35;
    y0=TP1;
    [t,y]=ode45(@(t,y)funS1(t,y,par),tspan,y0,opts);
    %compute re-entry x-location
    xcross(i)=findCrossAlpha(y,alpha);
    %compare re-entry point to location of pseudo-saddle
    if xcross(i)≥ 0
        if EqSig3(1)> xcross(i)
            text{i}='Left';
        elseif EqSig3(1)== xcross(i)
            text{i}='0';
        else
            text{i}='Right';
        end
    else
        text{i}='error';
    end
end
text'
```

Figure 46: Script pseudo-homoclinic connections 1

```
clear all
%parameters
a=0.3556;
b=0.33;
d=0.0444;
Ee=0.2067;
%exact value of bifurcation
alphaPSN=(b+1)^2/(4*a);
alphaBF=b*(a-b*d-d)/((a-d)^2);
%store parameters in vector to pass to ode45
par(1)=a;
par(2)=b;
par(3)=d;
par(4)=Ee;
%initialize loop variables
nloop=100;
alpha=1.24;
sign=-1;
epsi=10^(-1);
flag=1;
%initialize vectors
xEqSig3list=zeros(1,nloop);
xcross=zeros(1,nloop);
relerror=zeros(1,nloop);
alphalist=zeros(1,nloop);
relerror(1)=1;
opts = odeset('RelTol',1e-12);
for k=1:nloop
    %tangent point
    TP1=[(b*d)/(a - d), alpha];
    %find pseudo-equilibria
    SigDynamPoly = [1 b-1 a*alpha-b];
    roots1 = roots(SigDynamPoly);
    EqSig3=[roots1(2),alpha];
    xEqSig3list(k)=EqSig3(1);
    %solve the ode
    tspan=0:0.001:35;
    y0=TP1;
    [t,y]=ode45(@(t,y)funS1(t,y,par),tspan,y0,opts);
    %compute re-entry x-location
    xcross(k)=findCrossAlpha(y,alpha);
    %check if xcross lies left then to the right of saddle
    if k>1 && xEqSig3list(k-1) > xcross(k-1) && xEqSig3list(k) < ...
       xcross(k)
        epsi=0.5*epsi;
        sign=1;
    %check if xcross lies right then to the left of saddle
    elseif k>1 && xEqSig3list(k-1) < xcross(k-1) && xEqSig3list(k) ...
       > xcross(k)
        epsi=0.5*epsi;
        sign=-1;
    end
    %store alpha in list
    alphalist(k)=alpha;
    %error estimate
    if k>1
    relerror(k)=alphalist(k-1)-alphalist(k);
    end
    %update alpha
    alpha=alpha+sign*epsi;
    %termination criterion
    if alpha<alphaBF
        flag=0;
        break
    elseif abs(relerror(k))<10^(-12)
        break
    end
end
k
flag
alphaHC=alpha
```

Figure 47: Script pseudo-homoclinic connections 2